Chapter 6 Dynamic Mechanical Analysis

6.1 Introduction

The transport behavior of two series of penetrants, namely esters and alkanes in a polymeric adhesive, has been investigated by means of mass uptake and infrared experiments. Basic structure-property relationships between the molecular structure and chemical nature of a penetrant were derived. It is seen from Figure 1-1 that the structure of a penetrant strongly influences its transport and mechanical properties. Then, it is necessary to relate both the chemical structure and transport properties of these penetrants to their effects on mechanical properties of a polymer.

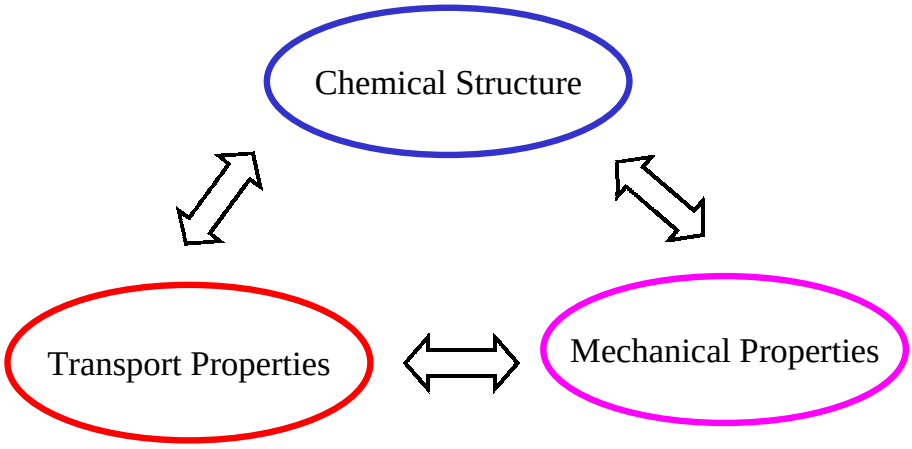

In this chapter, the effects of transport on the dynamic mechanical relaxation of the R/flex 410 polymeric adhesive are discussed. The presence of a low molecular weight has been known to drastically affect the mechanical relaxation of a polymeric system. Accelerated testing procedures based upon principles of time-temperature superpositioning proposed by Williams, Landel, and Ferry[1] were devised to create "doubly-reduced" master curves of the observed mechanical response. The diffusion phenomenon was introduced via the creation of a diffusion-time shift factor. This enabled the prediction of the dynamic mechanical response of the polymer as a function of temperature and exposure time to a penetrant based upon fundamental properties of both the penetrant molecule. Additional information regarding the molecular relaxation distribution and the effects of penetrant has also been discussed.

6.2 Background

Dynamic Mechanical Analysis

Dynamic mechanical properties refer to the response of a material as it is subjected to a periodic force. These properties may be expressed in terms of a dynamic modulus, a dynamic loss modulus, and a mechanical damping term. Typical values of dynamic moduli for polymers range from 10^6-10^{12} dyne/cm^2 depending upon the type of polymer, temperature, and frequency.

For an applied stress varying sinusoidally with time, a viscoelastic material will also respond with a sinusoidal strain for low amplitudes of stress. The sinusoidal variation in time is usually described as a rate specified by the frequency (f = Hz; ω = rad/sec). The strain of a viscoelastic body is out of phase with the stress applied, by the phase angle, δ. This phase lag is due to the excess time necessary for molecular motions and relaxations to occur. Dynamic stress, σ, and strain, ε, given as:

(1) $$\sigma = \sigma_o \sin(\omega t + \delta)$$

(2) $$\varepsilon = \varepsilon_o \sin(\varpi t)$$

where ω is the angular frequency. Using this notation, stress can be divided into an "in-phase" component ($\sigma_o \cos\delta$) and an "out-of-phase" component ($\sigma_o \sin\delta$) and rewritten as,

(3) $$\sigma = \sigma_o \sin(\omega t) \cos\delta + \sigma_o \cos(\omega t) \sin\delta.$$

Dividing stress by strain to yield a modulus and using the symbols E´ and E´´ for the in-phase (real) and out-of-phase (imaginary) moduli yields:

(4) $$\sigma = \varepsilon_o E' \sin(\varpi t) + \varepsilon_o E'' \cos(\omega t)$$

(5) $$E' = \frac{\sigma_o}{\varepsilon_o}\cos\delta \qquad E'' = \frac{\sigma_o}{\varepsilon_o}\sin\delta$$

(6) $$\varepsilon = \varepsilon_o \exp(i\omega t) \qquad \sigma = \sigma o \exp(\omega t + \delta)i$$

(7) $$E^* = \frac{\sigma}{\varepsilon} = \frac{\sigma_o}{\varepsilon_o} e^{i\delta} = \frac{\sigma_o}{\varepsilon_o}\left(\cos\delta + i\sin\delta\right) = E' + iE''$$

Equation (7) shows that the complex modulus obtained from a dynamic mechanical test consists of "real" and "imaginary" parts. The real (storage) part describes the ability of the material to store potential energy and release it upon deformation. The imaginary

(loss) portion is associated with energy dissipation in the form of heat upon deformation. The above equation is rewritten for shear modulus as,

$$G^* = G' + iG'' \tag{8}$$

where G′ is the storage modulus and G″ is the loss modulus. The phase angle δ is given by

$$\tan\delta = \frac{G''}{G'} \tag{9}$$

The storage modulus is often times associated with "stiffness" of a material and is related to the Young's modulus, E. The dynamic loss modulus is often associated with "internal friction" and is sensitive to different kinds of molecular motions, relaxation processes, transitions, morphology and other structural heterogeneities. Thus, the dynamic properties provide information at the molecular level to understanding the polymer mechanical behavior.

Time-Temperature Superposition

Due to the viscoelastic nature of polymeric materials, the analysis of their long-term behavior is essential. This has been the topic of many studies dealing with polymers.[2,3,4] For a viscoelastic polymer, the modulus is known to be a function of time at a constant temperature. The modulus is also a function of temperature at a constant time. According to this time-temperature correspondence, long term behavior of a polymer may be measured by two different means. First, experiments for extended periods of time can be carried out at a given temperature, and the response measured directly. This technique becomes increasingly time consuming due to the long response times of many polymers. The second method takes advantage of the principles of time-temperature correspondence wherein experiments are performed over a short time frame at a given temperature, and then repeated over the same time frame at another temperature. The two methods are equivalent according to the principles of time-temperature superpositioning.

These principles for studying long-term behavior of polymers have been well established by Williams, Landel, and Ferry[1], and have been eloquently explained and demonstrated by Aklonis and MacKnight[5]. The methods of time-temperature superpositioning (i.e. reduced variables) are used to accelerate the mechanism of a relaxation or molecular event by either increasing the temperature or increasing the stress, in the experiment. A classic example of such a procedure is given below[3] where the stress relaxation modulus from a tensile test is plotted as a function of time, over an accessible time scale, for various temperatures. A reference temperature of T_o=25°C was selected and the modulus-versus-time curves for the remaining isotherms were horizontally shifted towards this reference until an exact superposition is accomplished.

Shifting of each isothermal curve results in a much larger, smooth continuous curve known as a *master curve*. It can be seen that this procedure results in a dramatic increase in the range of the time scale. The inset below is known as the shift factor plot. The shift factor, a_T, represents the magnitude of shifting along the x-axis, necessary for a specific isotherm to superimpose on its neighbor in the final master curve with respect to a given reference temperature. The log a_T versus temperature plot should be a smooth monotonic curve, provided the mechanism of relaxation remains the same during the process. An inflection in the shift factor plot would be indicative of a change in the mechanism of the process, thus invalidating the procedure.

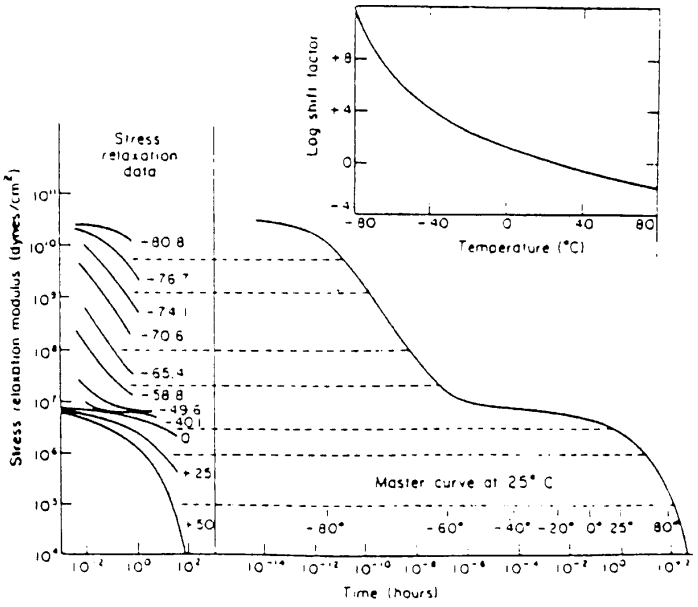

The actual graphical procedure can be mathematically described for a shifted isotherm T_1 as

$$E(T_o,t) = E(T_1, t/a_T) \tag{10}$$

This implies that the effect of changing temperature is the same as multiplying the time scale by a factor a_T, i.e., an additive factor to the log time-scale.

The criteria for the application of time-temperature superpositioning have been described in detail in Ferry's text[4]. The first criterion is that all adjacent curves should overlap over a reasonable number of data points. The second criterion is that the same values of the shift factor must translate all of the viscoelastic functions. Finally, the shift factor must follow one of the well-established relationships. The shift factor is usually described either by the WLF equation or the Arrhenius relationship. The WLF equation, named after its founders Williams, Landel, and Ferry[1], is described as

(11) $$Log\ a_T = \frac{-C_1(T - T_g)}{C_2 + (T - T_g)}$$

and is associated with the transition, plateau, and terminal regions of the time scale. The constants C_1 and C_2 are material dependent parameters that have been associated with fractional free volume and the empirical Doolittle expression, and are defined as B/2.303 f_g and f_g/α_f, respectively. The values of C_1=17.4 and C_2=51.6°K were originally thought to be "universal" and are still widely used[5]. The glassy region of a polymer is accurately described by the second form of the shift factor, namely the Arrhenius form (Eq. (12)) where

ΔE = activation energy (kJ/mole)
R= gas constant
T= temperature (°K)
T_{ref} =reference temperature (°K).

(12) $$Log\ a_T = \frac{-\Delta E}{2.303 * R}\left(\frac{1}{T} - \frac{1}{T_{ref}}\right)$$

Povolo and Fontelos[6] proposed a very rigorous approach to determine whether or not tTSP is applicable to a set of experimental data by analyzing their relation to each by a scaling method. It was shown, through examples, how superpositioning of curves seemed apparent, when, in reality, the experimental curves did not lead to a scalar relationship.

Methods of accelerated testing may be applied to any variable that accelerates the process without changing the mechanism of the process being measured. Some common variables are temperature, frequency, rate, humidity, filler content, pH and chemical polarity.

The use of *multiple* shifting variables, such as temperature and composition, may also be used to create a "doubly-reduced" master curve. As in the previous descriptions, it is necessary that the variables do not alter the mechanism of the process monitored. It is also imperative that the variables of interest are additive *only* and are independent of each other.

Multi-variable shifting has been utilized in the evaluation of stress-strain data for a butadiene elastomer by changing temperature and filler content.[7] Values of initial Young's moduli and of the ultimate properties-stress at break, strain at break, and the strain energy density-were evaluated at different temperatures and strain rates, and were all superimposed using the WLF equation with C_1=8.86 and C_2=101.6 and a reference temperature of –25°C. A double reduction in variables was done using an analogous form of the WLF equation for filler volume fraction, to create a single master curve. This allowed the prediction of stress-strain behavior as a function of both temperature and filler content. Differences in the apparent activation energy terms obtained from shifting the initial modulus and from shifting the ultimate properties were assumed to be a

measure of the interfacial strength between the polymer and filler surface. This composite strength increased greatly as the filler content increased. Values of the initial moduli proved to be dependent only upon filler content, since changes in filler particle size showed no effect. However, this generalization did not apply to the ultimate properties in which case dewetting occurred. The extent of dewetting was greater for larger filler particles than for smaller ones.

A similar study was also performed by Sumita *et al.*[8] on nylon 6 with varying contents of ultrafine fillers. The yield stress was evaluated at different rates as a function of temperature and filler content. Temperature shift factors for both the neat and filled systems exhibited an Arrhenius behavior, with a transition coinciding with a crystal transition of Nylon 6. Doubly-reduced master curves of yield stress were created for filler compositions ranging from 0% to 20%, indicating that the effects of strain rate and filler content were interconvertable with regard to yield stress. Resulting values of yield stress were interpreted in terms of the dispersion strength theory to describe the effects of filler size and content.

Another type of compositional shift factor was utilized in a study of semicrystalline poly(vinyl alcohol) and nylon 6[9]. Stress relaxation tests were performed in tension on both materials with different degrees of crystallinity, over a range of temperature (22°C to 77°C) and humidity. Log E(t) versus time curves could be shifted along the time axis using temperature and relative humidity as variables. Superposition of the variables was valid except for in the extremes of very high and low humidities and temperatures. This study concluded that the application of time-moisture superposition was valid when temperature conditions were near those of the polymer transition region.

Temperature and moisture were also used as shift variables in the analysis of low molecular weight poly(vinyl acetate) by Emri and Ravsek.[10] Samples were tested in torsion at temperatures from 20°C to 36°C and moisture contents of 0% to 3% water. Doubly reduced master curves demonstrated the application of time-moisture superposition of PVAc for the conditions given.

Kohan[11] has also shown the temperature-humidity equivalence for the yield stress of various nylons (nylon-6, -66, -610). Temperatures were varied from –40°C to 100°C, and humidity levels tested ranged from 0% to 100%. Each of the polymers showed similar trends in behavior with regard to temperature and humidity. However, the extent to which the relative humidity affected the yield stress varied from polymer to polymer. For instance, the properties of dry nylon-610 were similar to those of nylon-66 at 50% relative humidity. Unfortunately, no interpretation of the different humidity dependencies was made in terms of the individual polymer structures.

A very in-depth look at the application of reduced-variables to the composition of plasticizers within a polymer was undertaken by Schausberger and Ahrer[12]. The materials utilized in this study were two grades of polystyrene (M_w=385 kg/mole; M_w=2540 kg/mole). Two commercially available plasticizers, dioctyl sebacate and dioctyl phthalate, and one oligomeric-like 1,2-diphenylethane were incorporated into the

polystyrene samples in compositions ranging from 0% to 25% weight. Frequency-temperature master curves of the dynamic shear storage and loss moduli were constructed for the two neat polymers, with reference temperatures of 160°C and 180°C, respectively. Additional frequency-temperature master curves were created for the polymers containing various compositions of plasticizer. The magnitude of relaxation strength was shown to depend upon the square of the weight fraction of the plasticizer. The WLF constant C_1 exhibited a decrease with increasing plasticizer content while C_2 increased with increasing plasticizer content. The dynamic moduli curves of varying plasticizer concentrations could be superimposed on each other. All curves were shifted along the log(frequency) axis to a reference curve of zero concentration, and the number of log(frequency) units translated was designated as a *concentration shift factor*. These concentration shift factors were observed to roughly follow a power law relationship with the weight fraction of plasticizer. A more accurate description of the relationship between plasticizer concentration and the concentration shift factor was given by a generalized free volume model of Fujita and Kishimoto[13], in which polymer-diluent interactions were ignored. This model was extended to describe the effect of the plasticizer on decreasing the number average molecular weight of the system. The use of shear geometry was very important in this analysis, since any heterogeneity within the polymer-diluent system would be, in a sense, "averaged out" during the experiment. Furthermore, the actual shear testing arrangement minimized the surface area through which a diluent could evaporate out of the sample. Using this procedure, the loss of any diluent due to evaporation, was observed to be negligible.

Recent work by Shepherd and Wightman[14] on a silicone adhesive sealant investigates the effects of temperature and relative humidity on the sealant peel fracture energy from a number of different substrates. Doubly reduced master curves were constructed, allowing the prediction of crack growth rates as a function of fracture energy, temperature, and relative humidity of the silicone sealants.

The above discussion demonstrates the utility of multiple shifting variables based upon the principles of time-temperature superpositioning in a variety of applications. The current study attempts to extend the concept of a compositional shift factor to incorporate the kinetic process of diffusion. The concept of a "*diffusion time shift factor*" will be introduced to correlate the observed mechanical properties with the diffusion process. This, in conjunction with the temperature shift factor allows for prediction of the mechanical properties of the adhesive as a function of temperature and diffusion time, *simultaneously*.

6.3 Concept of Distribution of Relaxation Times

The concept of relaxation time as it applies to polymeric materials has been described in many texts[5,15,16,40]. Typical response of a polymeric material can not be described accurately with a "single relaxation time" unlike that of a liquid material. This inability to be described by a single relaxation time is a result of its viscoelastic nature and is one of the characteristics that give polymers their unique properties. In order to demonstrate the concept of "multiple relaxation times" for polymers, it is necessary to describe the development of this concept from the fundamental theories from which it originated. McCrum *et al*.[40] and T. Park[17] have both given a very thorough description of this development. Based upon their reviews, two basic categories of models describing single and multiple relaxation times will be discussed below.

The most simple relaxation model is that described by Debye via molecular modeling.[18] The time decaying function in the Debye model is described by the following exponential:

$$\Phi(t) = \exp\left(\frac{-t}{\tau}\right) \tag{13}$$

where $\Phi(t)$ is the decay function and τ is the *single* relaxation time. Based upon this model, equations such as the one shown below may be derived to permit fitting of experimental data to evaluate the relaxation time τ.

$$\frac{\varepsilon^* - \varepsilon_\infty}{\varepsilon_s - \varepsilon_\infty} = \frac{1}{1 + i\omega t} \tag{14}$$

where ε^* is the complex dielectric constant
ε_s = the relaxed dielectric constant, and
ε_∞ = the unrelaxed dielectric constant.

In simple terms, ε_s and ε_∞ can be described as the dielectric constants at very low and very high frequencies, respectively. Their difference is directly, $(\varepsilon_s - \varepsilon_\infty)$, is directly related to the relaxation strength. The previous expressions of the Debye model, like many of the following empirical models, were originally formulated for dielectric properties. However, in the current study, the primary concern is the study of dynamic mechanical relaxations in a shearing mode of testing. Fortunately, the development of relationships for dynamic mechanical relaxation parallels that of dielectric relaxation[40]. So, the mechanical analogue of equation (14) described above, is given by:

$$\frac{G^* - G_\infty}{G_s - G_\infty} = \frac{1}{1 + i\omega t} \tag{15}$$

All ensuing relationships describing the development of relaxation models will be described in terms of shear moduli (G).

This model is far from being able to accurately describe the broad relaxation range of polymers. However, as will be seen, it forms the basis for other more accurate empirical models for describing the relaxation distribution.

Advances in more accurately describing the relaxation distribution of polymers were made in the work of Cole and Cole[19]. These researchers described the response of a polymer to a stress in terms of multiple relaxation times. The time decaying function for a *multiple* relaxation model was assumed to be a *linear summation* of the time decaying function for a *single* relaxation model (equation(16)).

$$\Phi(t) = \sum_i A(\tau_i)\exp^{\left(\frac{-t}{\tau_i}\right)} \tag{16}$$

where $A(\tau_i)$ is the fraction of a single relaxation time mechanism with relaxation time τ_i. Based upon the Cole-Cole model, it has been shown[17,19] that the expression describing dynamic mechanical data may be written as:

$$\frac{G^* - G_\infty}{G_s - G_\infty} = \frac{1}{1+(i\omega\tau_o)^{1-\alpha}} \tag{17}$$

where τ_o is considered as a central relaxation time about which all other relaxation times are distributed, and α is a fitting parameter with limits of $0 \leq \alpha \leq 1$. This equation reduces to the Debye expression for $\alpha=0$, as can be seen by comparison with equation (15). As the deviation from a single relaxation time model becomes greater, $\alpha \Rightarrow 1$, the dispersion becomes broader than that for a single relaxation time, but remains symmetrical about $\omega\tau_o=1$. Cole and Cole[19] proposed a method of graphically representing the effects of multiple relaxation times, which now bears their name. A Cole-Cole plot consists of constructing an Argand diagram, or complex plane plot, in which G″ is plotted against G′. The expression derived by them can be expressed as:

$$\left[G' - \frac{G_s + G_\infty}{2}\right]^2 + \left[G'' + \frac{(G_s - G_\infty)}{2}\cot an\frac{(1-\alpha)\pi}{2}\right]^2 = \left[\frac{(G_s - G_\infty)}{2}\cos ec\frac{(1-\alpha)\pi}{2}\right]^2 \tag{18}$$

This model represents a depressed semi-circle whose center is below the abscissa as shown in Figure 6-1. Increasing deviation from a single relaxation time is represented by a depression of the semi-circle. Values for τ_o and α can be found experimentally using the following expressions.

(19) $$\frac{G'(\omega)-G_\infty}{G_s-G_\infty}=\frac{1+(\omega\tau_o)^{1-\alpha}\sin(\alpha\pi/2)}{1+2(\omega\tau_o)^{1-\alpha}\sin(\alpha\pi/2)+(\omega\tau_o)^{2(1-\alpha)}}$$

(20) $$\frac{G''(\omega)}{G_s-G_\infty}=\frac{(\omega\tau_o)^{1-\alpha}\cos(\alpha\pi/2)}{1+2(\omega\tau_o)^{1-\alpha}\sin(\alpha\pi/2)+(\omega\tau_o)^{2(1-\alpha)}}$$

The Cole-Cole empirical equations describe dispersion and absorption curves as being symmetrical about the position $\omega\tau_o=1$. However, the behavior of real polymers is characterized by loss curves with a high frequency broadening. Modification of the Cole-Cole model was proposed by Davidson and Cole[20] in order to encompass the "skew" in the Cole-Cole arcs. Incorporation of this concept resulted in the following empirical equations:

(21) $$\frac{G^*-G_\infty}{G_s-G_\infty}=\frac{1}{(1+i\omega\tau o)^\gamma}$$

(22) $$\frac{G'(\omega)-G_\infty}{G_s-G_\infty}=(\cos\phi)^\gamma\cos(\phi\gamma)$$

(23) $$\frac{G''(\omega)}{G_s-G_\infty}=\cos(\phi)^\gamma\sin(\phi\gamma)$$

where $\phi=\arctan(\omega\tau_o)$, and γ = a fitting parameter with the limits of $0 \le \gamma \le 1$. A Cole-Cole diagram of equations (22) and (23) demonstrates the prediction of a skewed distribution of relaxation times about τ_o (Figure 6-2). The smaller the value of γ, the more asymmetric the resulting semicircle becomes. As γ approaches 1, then the form of the Debye single relaxation model is re-gained.

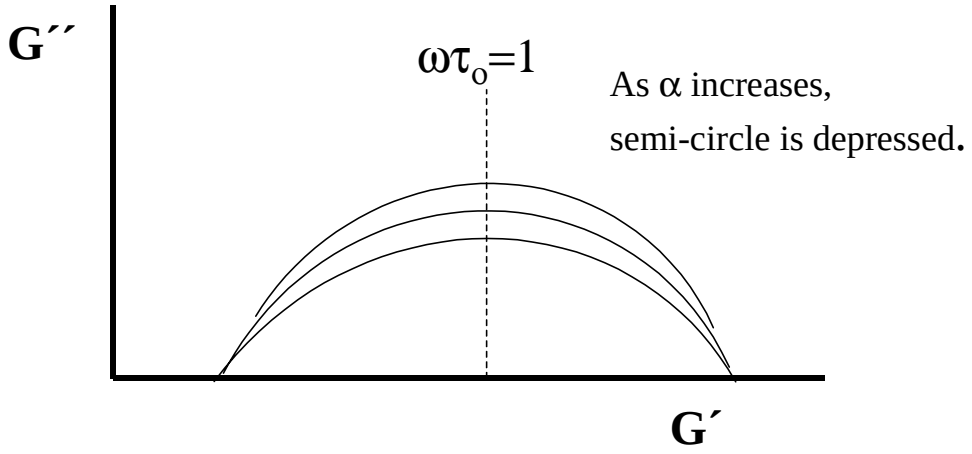

Figure 6-1: Schematic Plot of Cole-Cole Model

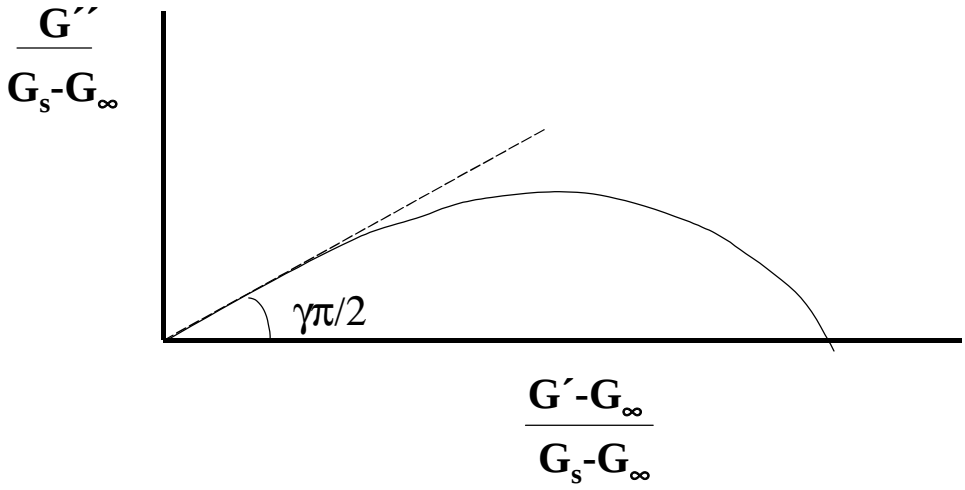

Figure 6-2. Schematic of Cole-Davidson Model

The Cole-Cole and Cole-Davidson models are empirical relationships that have been designed to fit experimental data by describing the symmetric and asymmetric relaxation time distributions. Both of them may be described as single parameter models. Havriliak and Negami[21] devised a two parameter empirical model that combined the concepts of both the Cole-Cole and Cole-Davidson models. The resulting Havriliak-Negami (H-N) empirical model is denoted as equation (24) in which the values of α and γ retain their original meanings from the Cole-Cole and Cole-Davidson models.

(24) $$\frac{G^* - G_\infty}{G_s - G_\infty} = \frac{1}{\left(1 + (i\omega\tau_o)^{1-\alpha}\right)^\gamma}$$

Park[17] has described the corresponding G′(ω) and G″(ω) relationships which were derived from the complex form of equation (24) as:

(25) $$G'(\omega) - G_\infty = r^{-\gamma/2}(G_s - G_\infty)\cos(\theta\gamma)$$

(26) $$G''(\omega) = r^{-\gamma/2}(G_s - G_\infty)\sin(\theta\gamma)$$

where $$r = \left((1 + (\omega\tau_o)^{1-\alpha}\sin(\alpha\pi/2)\right)^2 + \left((\omega\tau_o)^{1-\alpha}\cos(\alpha\pi/2)\right)^2$$

and $$\theta = \arctan\left(\frac{(\omega\tau_o)^{1-\alpha}\cos(\alpha\pi/2)}{1 + (\omega\tau_o)^{1-\alpha}\sin(\alpha\pi/2)}\right)$$

The (H-N) expressions are the most versatile empirical relationships due to the existence of two fitting parameters. Therefore, they have often been used to empirically fit dielectric data[17,22,23] as well as dynamic mechanical data[24]. The dynamic mechanical loss moduli determined experimentally in the current study will be fit in the frequency domain using the H-N formalism. A program that has been written by Park[17] will be utilized for this purpose, and is listed in Appendix F of this text.

A time decaying function is mathematically very difficult to derive based upon the Havriliak-Negami expressions. However, a methodology proposed by Boese and Kremer[22] involves the use of a Fourier transform of the general expression for dynamic relaxation response as shown below[25,26,27].

(27) $$\frac{G^* - G\infty}{Gs - G\infty} = \int_0^\infty \exp(-i\omega t)\left[-\frac{d\Phi(t)}{dt}\right]dt$$

The time domain and the frequency domain parts of equation (27) are described as equation (28) and equation (29), respectively.

(28) $$f(t) = -\frac{d\Phi(t)}{dt}$$

(29) $$g(\omega) = \frac{G'(\omega) - G_\infty}{G_s - G_\infty}$$

Since G′(ω) is an even function of ω, and G″(ω) is an odd function of ω, the respective Fourier transforms are as follows:

(30) $$-\frac{d\Phi(t)}{dt}=\frac{2}{\pi}\int_0^{\infty}\left(\frac{G'(\omega)-G_{\infty}}{G_s-G_{\infty}}\right)\cos(\omega t)d\omega$$

(31) $$-\frac{d\Phi(t)}{dt}=\frac{2}{\pi}\int_0^{\infty}\left(\frac{G''(\omega)}{G_s-G_{\infty}}\right)\sin(\omega t)d\omega$$

Expressions for the time decaying function $\Phi(t)$ are found by integration of equations (30) and (31), respectively. The resulting integrated expressions are given by:

(32) $$\Phi(t)=\frac{2}{\pi}\int_0^{\infty}\left(\frac{G_{\infty}-G'(\omega)}{G_s-G_{\infty}}\right)\frac{\sin(\omega\tau)}{\omega}d\omega$$

(33) $$\Phi(t)=\frac{2}{\pi}\int_0^{\infty}\left(\frac{G''(\omega)}{G_s-G_{\infty}}\right)\frac{\cos(\omega t)}{\omega}d\omega$$

Using equations (32) and (33), the time decaying function can be numerically evaluated from the modulus versus frequency data. The functional form of the H-N description has been used to evaluate the $G''(\omega)$ term in equation (33). Typical decay time functions evaluated in this manner are shown for the dielectric response of poly(hydroxybutyrate)[17] (PHB) at different temperatures (Figure 6-3).

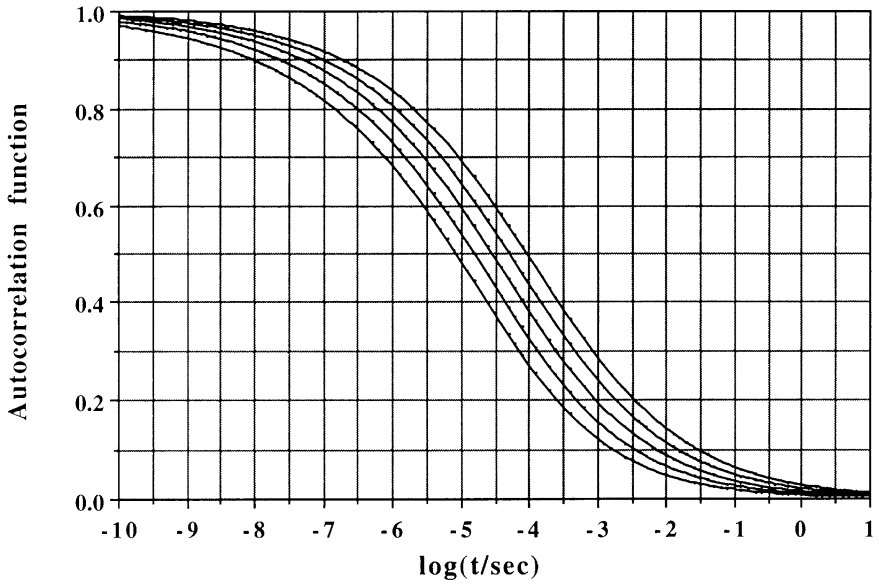

Figure 6-3. ACF for poly(hydroxybutyrate) at temperatures increasing from 25°C to 33°C (left to right) in increments of 2°C.

In the current study, time decaying functions for loss moduli versus frequency data have been evaluated using a program that is given in Appendix G[17], which is based upon the H-N formalism.

The time decay function created using the H-N parameters may be compared with the well-known Kohlrausch-Williams-Watts (KWW) function. The KWW function[28] is an empirical function that can describe the non-exponential time decaying behavior of many relaxation processes. It is described by the following expression:

$$\Phi(t) = \exp\left(-1\left(\frac{t}{\tau_o}\right)^{\beta}\right) \tag{34}$$

where τ_o is the time at which $\Phi(t)$ decays to 1/e and the exponent β describes the breadth of the distribution in the limits of $0 \leq \beta \leq 1$. It has been shown[29] that as β increases from 0 to 1, the distribution of relaxation times changes from a broad, symmetric distribution to a sharp, asymmetric one. The KWW decay function has become widely used to model many relaxation processes in polymers[30,31,32]. The β term has been associated with a coupling parameter, $n=1-\beta$, describing the degree of intermolecular cooperativity associated with a relaxation process[30,31,33].

In the current study, KWW expression (equation (34)) has been fit to the time decay function created using the H-N parameters to evaluate τ_o and β for the dynamic

mechanical response observed experimentally. Fitting of equation (34) has been done using a non-linear program detailed in Appendix H[17].

The concept of a *mean relaxation time* is a useful parameter that can describe and compare the *average* relaxation behavior of different materials. It has been shown[17,34] that an expression for the mean relaxation time can be deduced from the KWW expression as:

$$(35) \qquad <\tau>=\int_0^\infty \exp\left(-1\left(\frac{t}{\tau}\right)^{\beta}\right)dt$$

By substituting $X=(t/\tau_o)^{\beta}$,

$$(36) \qquad <\tau>=\frac{\tau_o}{\beta}\int_0^\infty \exp(-X)X^{\left(1/\beta\right)-1}dX$$

which can be re-written as the following *gamma* function:

$$(37) \qquad <\tau>=\frac{\tau_o}{\beta}\Gamma\left(\frac{1}{\beta}\right)$$

Equation (37) is the expression that will be used for evaluating mean relaxation times, $<\tau>$, for each of the polymer dynamic mechanical experiments in the current study. The mean relaxation times will be evaluated as a function of exposure time to different solvents. Together, all of the parameters described above will be utilized to investigate the effects of solvent and exposure time on the relaxation behavior of the R/flex 410 adhesive system. Particular attention will be paid to the β parameter of the KWW function to describe the changing cooperative nature of the relaxation process.

6.4 Temperature-Frequency Master Curves

As described earlier in this study, the mechanical properties of the Rogers R/flex 410 adhesive have been tested dynamically using a "sandwich" shearing geometry. This particular testing mode and geometry were chosen due to the low T_g and poor structural rigidity of the material. Dynamic mechanical data at temperatures in increments of 3°C ranging from –65° to 280°C has been obtained. A total of eight frequencies (0.1, 0.3, 1,3, 10,30, 50, and 100 hz) were swept at each temperature.

Samples were exposed to the penetrants for various times ranging from 1 to 10^5 minutes at room temperature. Then, they were weighed, their thicknesses were measured and they were placed between the shear plates. The plates were clamped intimately to the surface of the samples so as to insure contact and to minimize penetrant evaporation. An excess of penetrant was also placed inside the testing chamber to lower the penetrant activity within the sample. Samples were quickly cooled down to -65°C and then heated to the final temperature of 280°C. The transition of interest for the neat polymer was ≤ 32°C, and the boiling points of most penetrants were ≥ 100°C. Thus, the majority of penetrant remained within the sample as confirmed by measuring the penetrant mass at T > 50°C during the course of an actual experiment.

Dynamic mechanical data was collected on these samples and their loss modulus, G''(ω), was plotted as a function of log(frequency). A representative plot for a polymer exposed to decane for 10^5 minutes is shown in Figure 6-4. This sample was designated as Decane-100K after the penetrant used and the time of exposure. For purposes of brevity, such a designation is used throughout the remainder of this text.

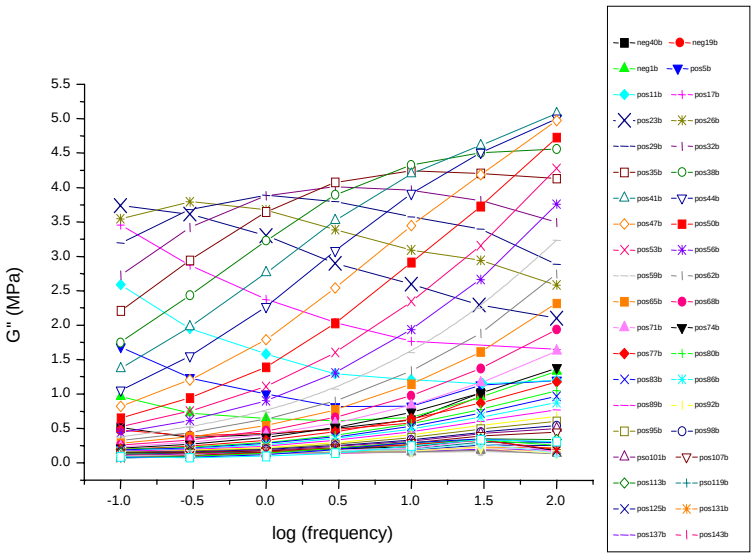

Figure 6-4. Dynamic loss moduli as a function of frequency for polymer sample exposed to decane penetrant for 10^5 minutes

Each experiment consisted of a data set of approximately 60 isothermal curves. The concept of time-temperature superpositioning (tTSP) was used to create a frequency-temperature master curve for the sample. Each isotherm was shifted left or right along the log frequency axis relative to a reference isotherm in order to achieve maximum overlap of the data. The reference isotherm was chosen as T_{ref}=50°C which is approximately the peak position of the middle-most frequency (3hz) for the neat material. Shifting was done so as to ensure that each curve matched the slope of its immediate neighbor, closest to the reference curve. The number of log (frequency) units through which an isotherm was translated is termed as its temperature-shift factor and is designated as $log\ a_T$. By convention, shifts towards the right are designated as negative while those towards the left are positive shifts

Horizontal shifting essentially compensated for a change in the time scale of a process induced by changes in temperature. It is known from the thermo-mechanical spectrum of polymers that a change in modulus co-exists with a change in temperature, and that thermal expansion decreases the amount of material per unit volume. Since modulus is defined per unit area, deviations from purely horizontal shifting may be due to both of the above factors. These deviations are manifested in the form of a vertical shift that involves translation of the isothermal curves along the modulus-axis. It is often rectified by normalizing moduli by the changing density and temperature as:[5,35]

(38) $$E(T_1,t) / \rho(T_1)\ T1 = E(T_2,t/a_T) / \rho(T_2)\ T_2$$

In the current study, vertical shifting was used only when absolutely necessary and their magnitudes were very small as can be seen from a few examples in Appendix K. An example of the final master curve for a sample exposed to the penetrant decane for 10^5 minutes is shown in Figure 6-5. The corresponding shift factor plot is given in Figure 6-6 and shows a smooth transition with no discontinuities. It follows the general shape expected from the theories of Williams, Landel and Ferry[1]. The low temperature tail of this plot exhibits an inflection due to the failure of tTSP at lower temperatures ($T \leq T_g$) and not from any effects due to penetrant melting as shown in DSC scans also given in Appendix K.

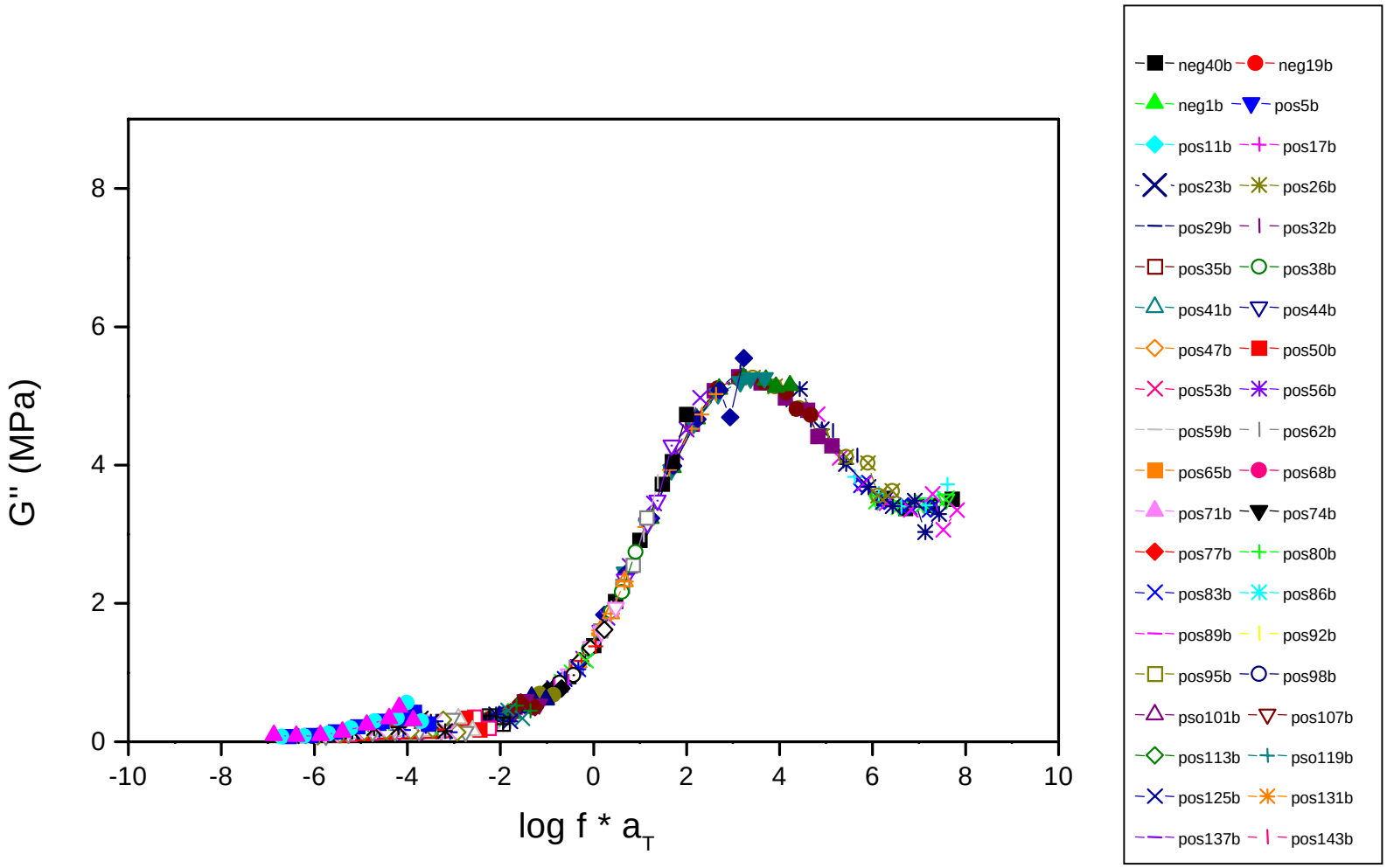

Figure 6-5. Frequency-temperature master curve of polymeric adhesive after exposure to decane for 10^5 minutes

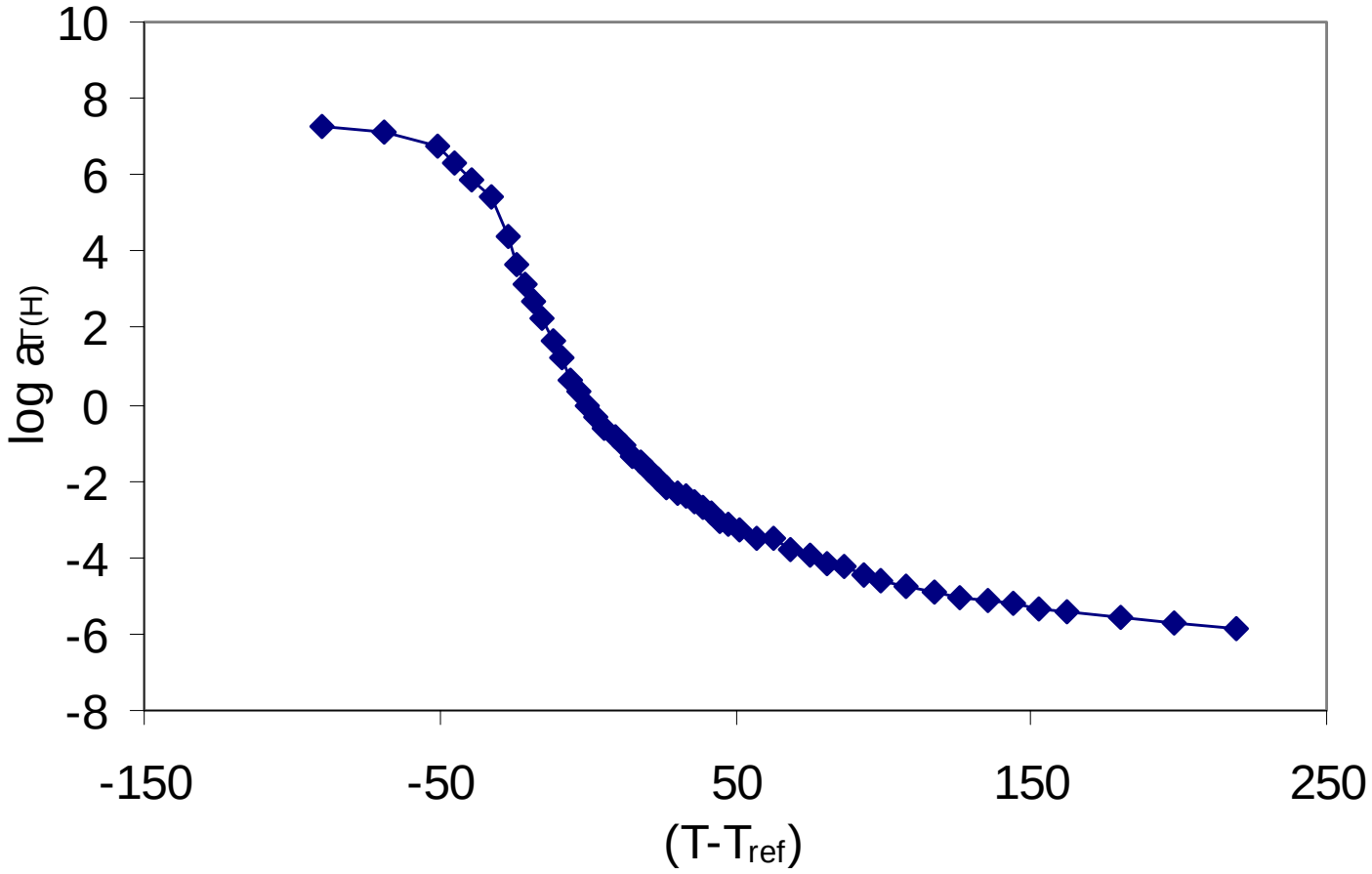

Figure 6-6. Temperature-shift factor plot for polymeric adhesive exposed to decane for 10^5 minutes. C_1 and C_2 values are 8.03 and 76.0, respectively.

In Figure 6-5, the breadth of the loss modulus master curve indicates the broad spectrum of relaxation times due to the crosslinked nature of the polymer.[36] Using frequency-temperature superpositioning, the range of frequencies has now been expanded by a factor of at least 3 decades. This enables a prediction of the material response at various frequencies, usually unobtainable experimentally.

The data presented in Figure 6-5 and Figure 6-6 are representative of only one penetrant at one exposure time. However, the polymeric adhesive was exposed to each of the nine *n*-alkane penetrants and each of the nine ester penetrants, for up to six decades of time (10^0-10^5 min). The master curves were constructed using frequency-temperature superpositioning for each of these penetrants and each of the exposure times. It is not possible to show all these master curves in this text for purposes of brevity. However, a few typical master curves and their corresponding shift factor plots are shown in the following pages (Figure 6-7 through Figure 6-20).

The general form for the WLF equation has been described earlier as

$$\log a_T = \frac{-C_1\left(T - T_g\right)}{C_2 + \left(T - T_g\right)} \tag{39}$$

Comparison to the empirical Doolittle equation, and an assumption of a linear expansion of free volume above T_g, provides physical significance to the constants, C_1 and C_2. C_1 can be given by $B/2.303\, f_g$, and C_2 by f_g/α_f, where B is the Doolittle constant and f_g is the fractional free volume at T_g. Thus, C_1 and C_2 values can describe the state of a material, in relation to its free volume. So, changes in free volume are reflective of changes at the molecular level. C_1 and C_2 constants may be found experimentally using a linearized form of the WLF equation. Based upon this linearized form, a plot of $-1/\log a_T$ versus $1/(T-T_{ref})$ yields a y-intercept equal to $1/C_1$ and a slope proportional to (C_2/C_1). Example plots of this analysis are given in Appendix K, and tables of all C_1 and C_2 values for each of the penetrants and exposure times are given in Table 6-1 through Table 6-18. The quality of the fits were excellent with statistical R^2 values greater than 0.98. There is no clear trend in the values of C_1 and C_2 determined for each penetrant and exposure time. This result may be due to the range of data selected for the WLF constant evaluation. Regression of the data was limited to the range between T_{ref} and (T_{ref}+100°C) due to the validity of the WLF equation in this temperature regime, and the fact that gross deviations from WLF behavior were observed in the shift factor plots at temperatures far below Tg.

One question that needs to be addressed results from the complex nature of the diffusion process, itself. During transport of a penetrant into a polymer film, a time-dependent gradient in concentration exists throughout the thickness of the film. In this analysis, all dynamic mechanical properties are assumed to be "average" values from the entire thickness of the films (i.e. homogenous distribution of penetrant). This assumption is valid since the shear geometry of the test yields information resulting more from the entire thickness of the film. Also, additional experiments were performed to see whether

or not the observed mechanical response is affected by concentration gradients. Polymer films were exposed to different penetrants and exposure times. They were then removed from the liquids and promptly sealed in airtight containers for various lengths of time (up to one month) for penetrant to equilibrate and become homogeneously distributed. Dynamic mechanical tests were then performed and results from the equilibrated and un-equilibrated films corresponded extremely well, as can be seen from some examples given in Appendix K.

Each set of experimental data superimposed very well to form a smooth master curve using temperature as the shift variable. As mentioned earlier, the magnitude of vertical shifting employed was very small. The horizontal shift factor plots (log a_T vs. $(T-T_{ref})$) also formed smooth functions of the WLF form. Each shift factor plot enables the prediction of the resulting master curve of the material response, at a different reference temperature.

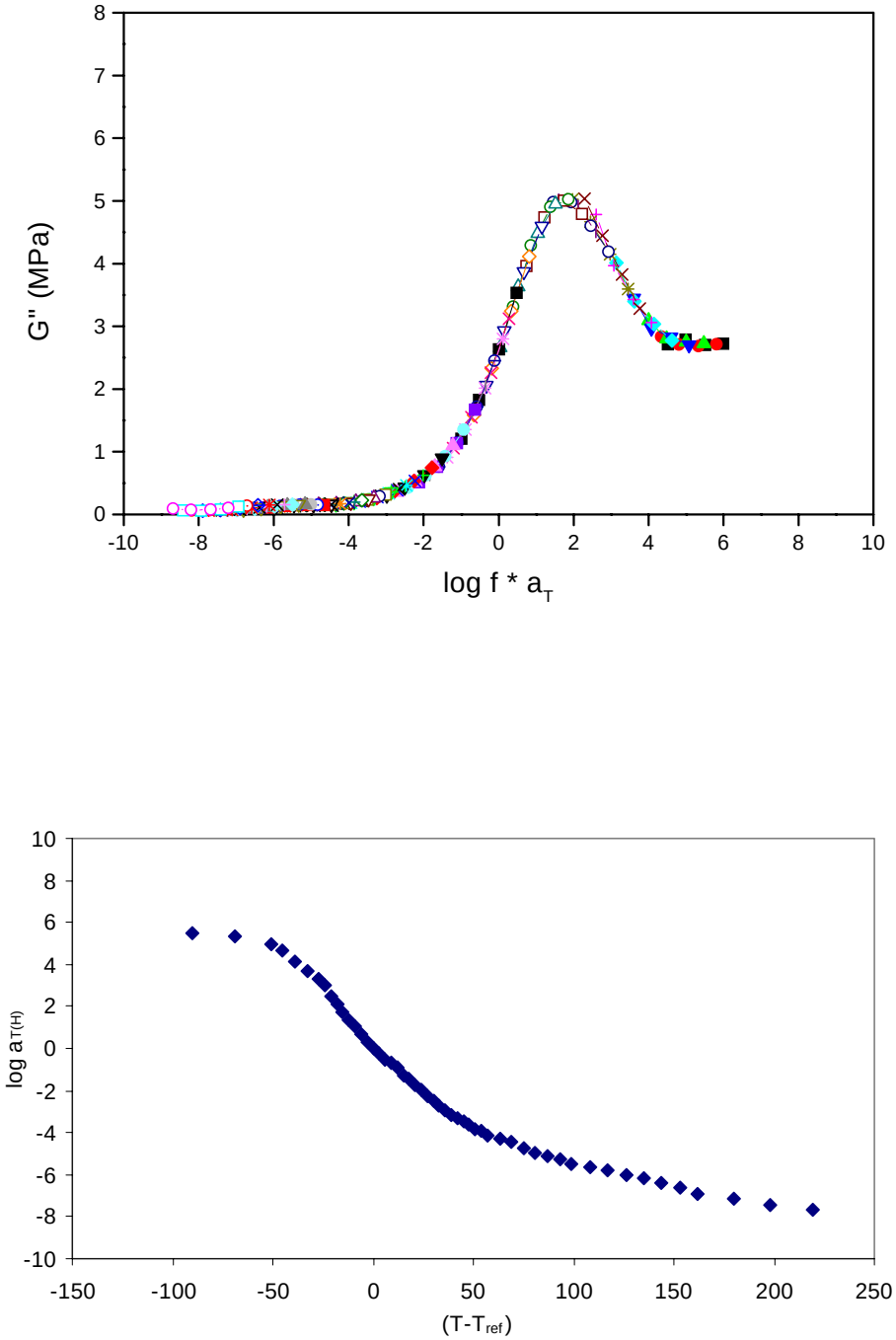

Figure 6-7. Frequency-temperature dynamic loss modulus master curve and the corresponding temperature shift-factor plot of adhesive exposed to *decane* penetrant for 10^2 minutes. (legend same as in Figure 6-5)

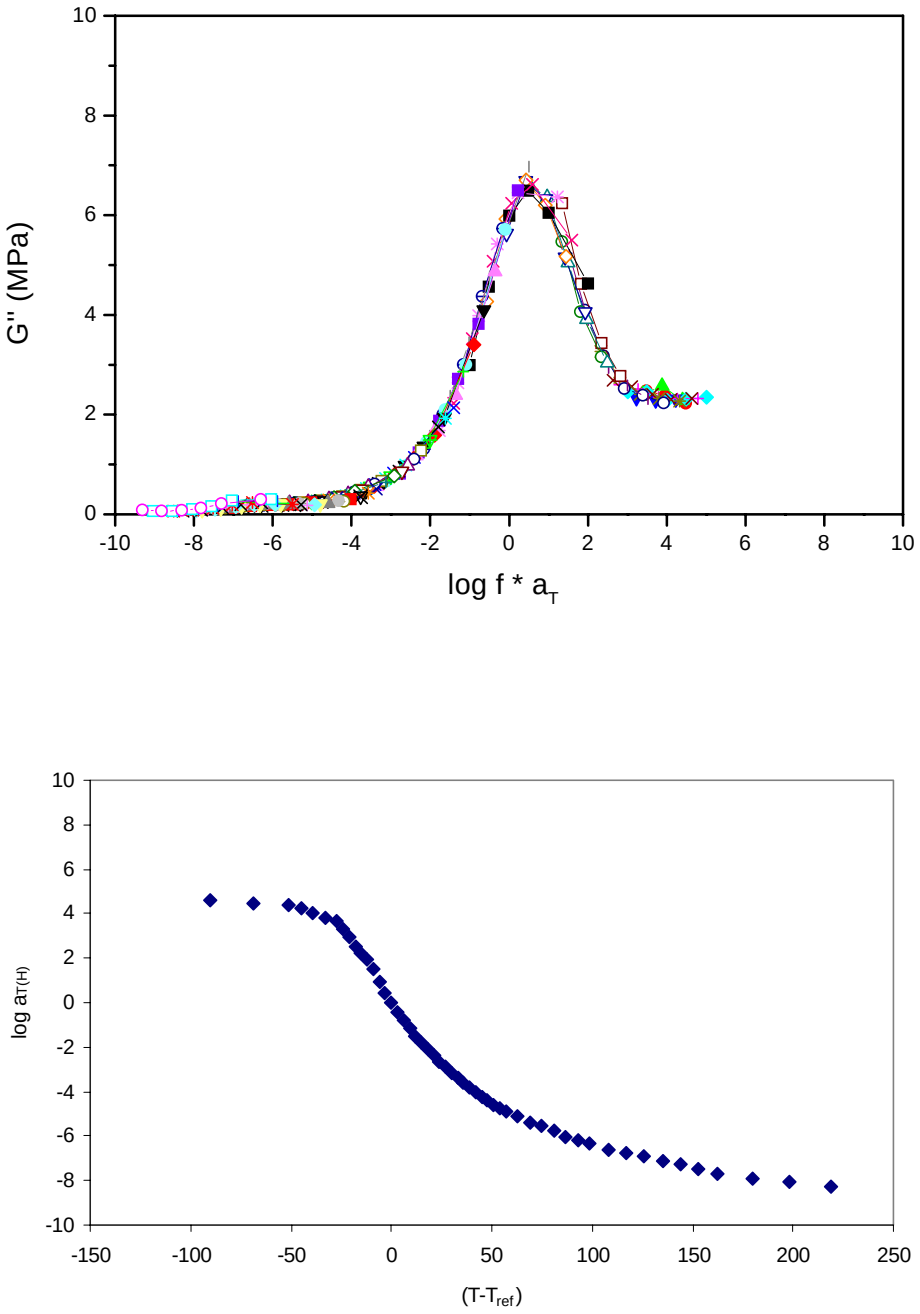

Figure 6-8. Frequency-temperature dynamic loss modulus master curve and the corresponding temperature shift-factor plot of adhesive exposed to *decane* penetrant for 10^0 minute. (legend same as in Figure 6-5)

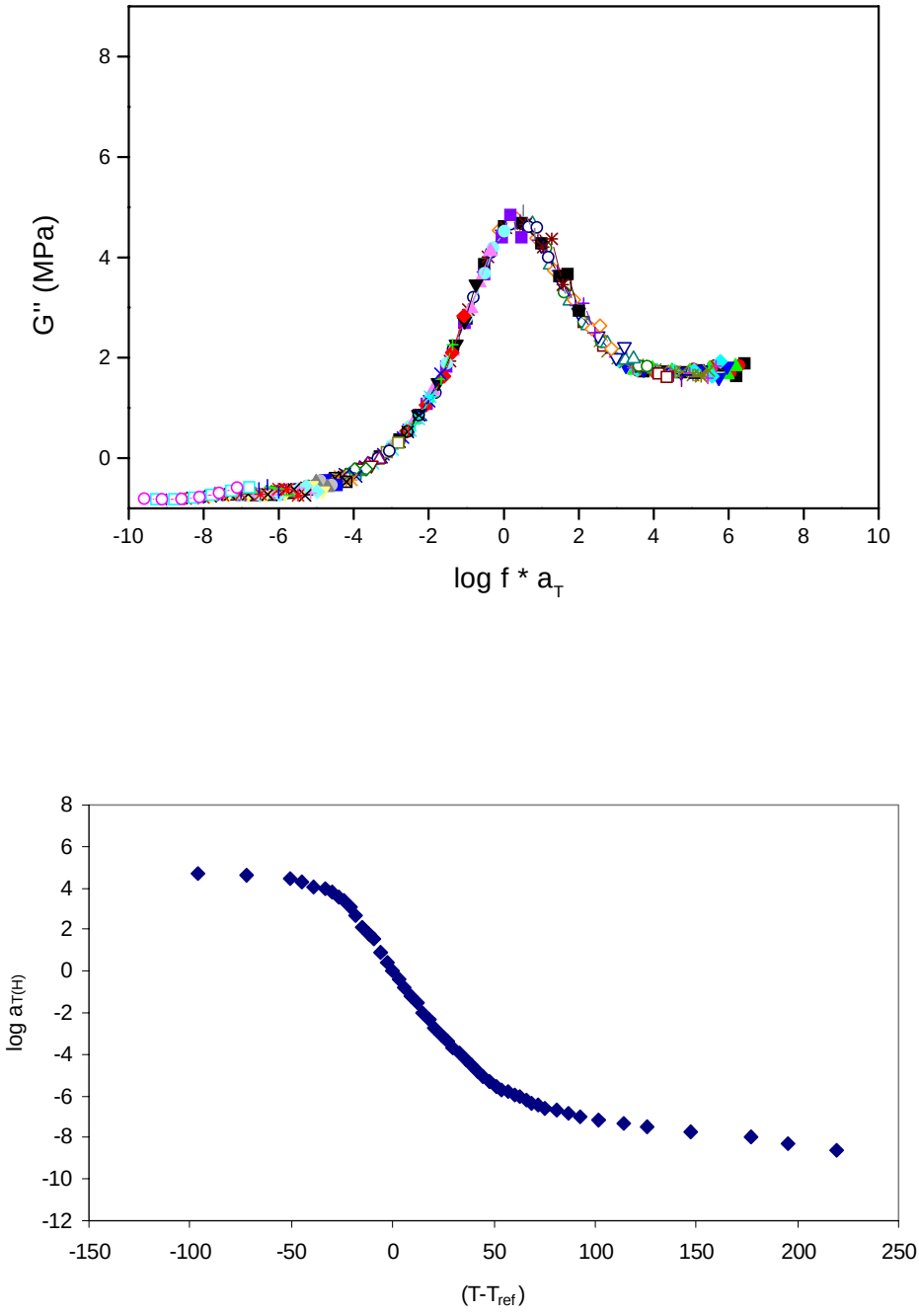

Figure 6-9. Frequency-temperature dynamic loss modulus master curve and the corresponding temperature shift-factor plot of adhesive exposed to *tridecane* penetrant for 10^1 minutes. (legend same as in Figure 6-5)

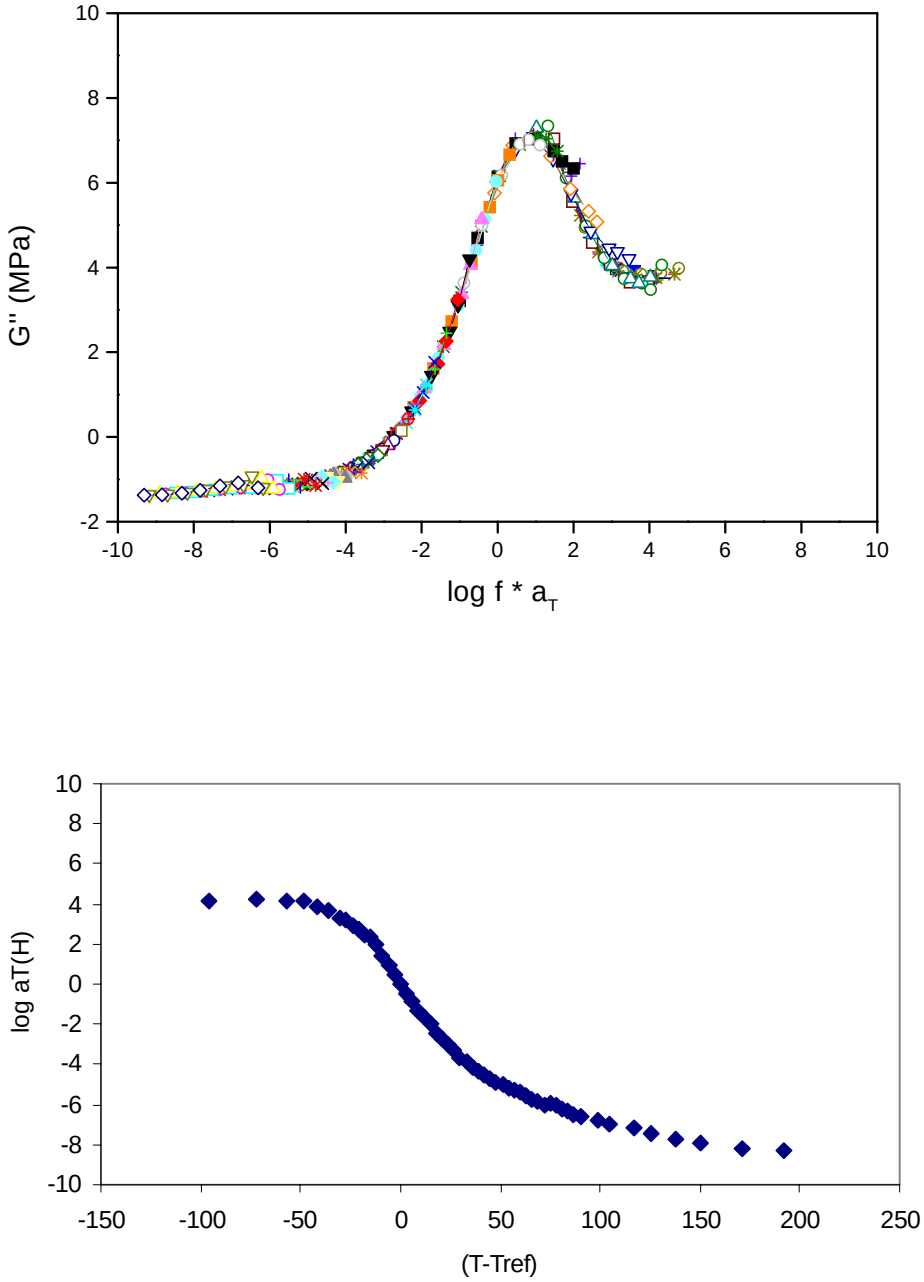

Figure 6-10. Frequency-temperature dynamic loss modulus master curve and the corresponding temperature shift-factor plot of adhesive exposed to *tridecane* penetrant for 10^3 minutes. (legend same as in Figure 6-5)

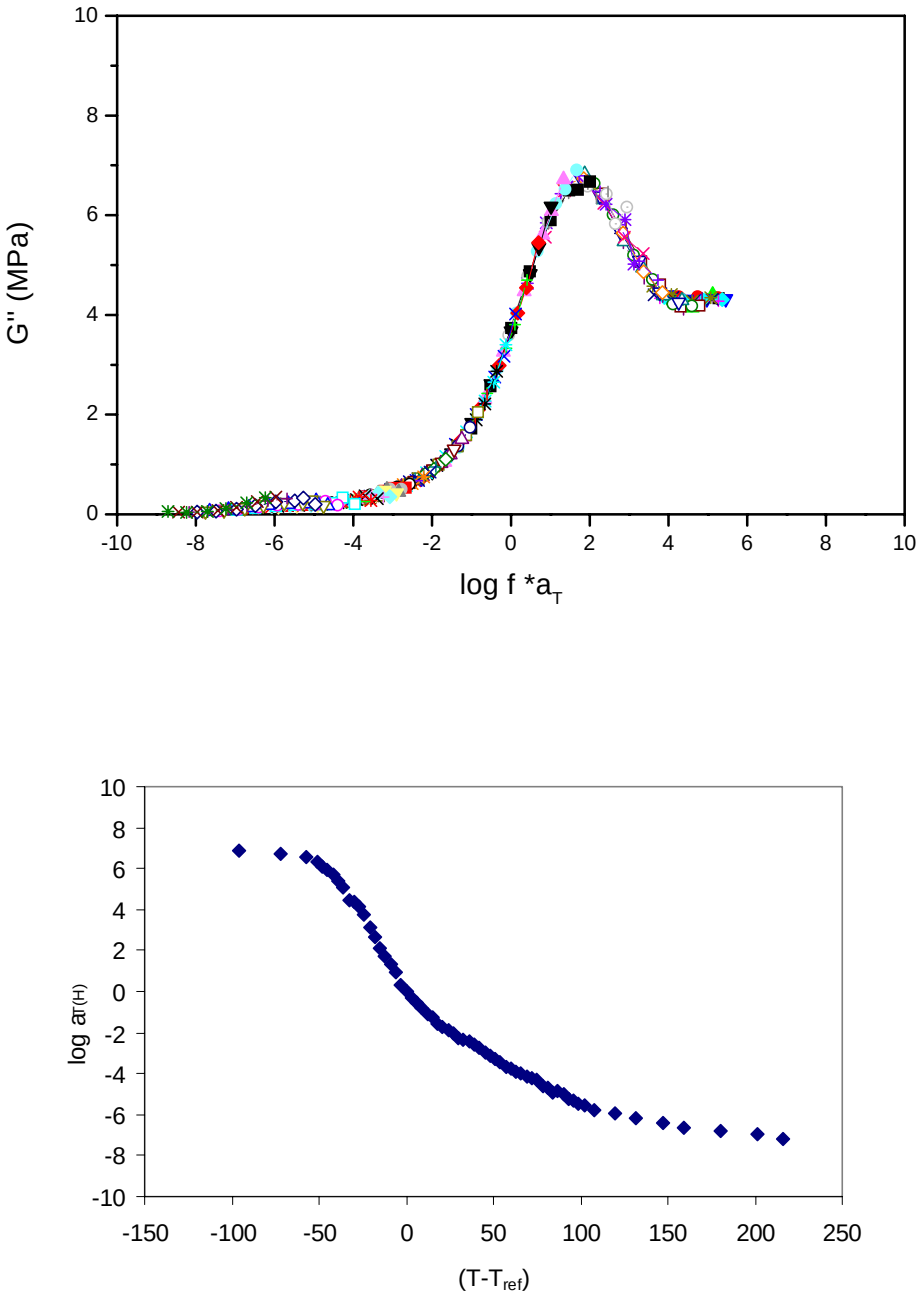

Figure 6-11. Frequency-temperature dynamic loss modulus master curve and the corresponding temperature shift-factor plot of adhesive exposed to *tridecane* penetrant for 10^5 minutes. (legend same as in Figure 6-5)

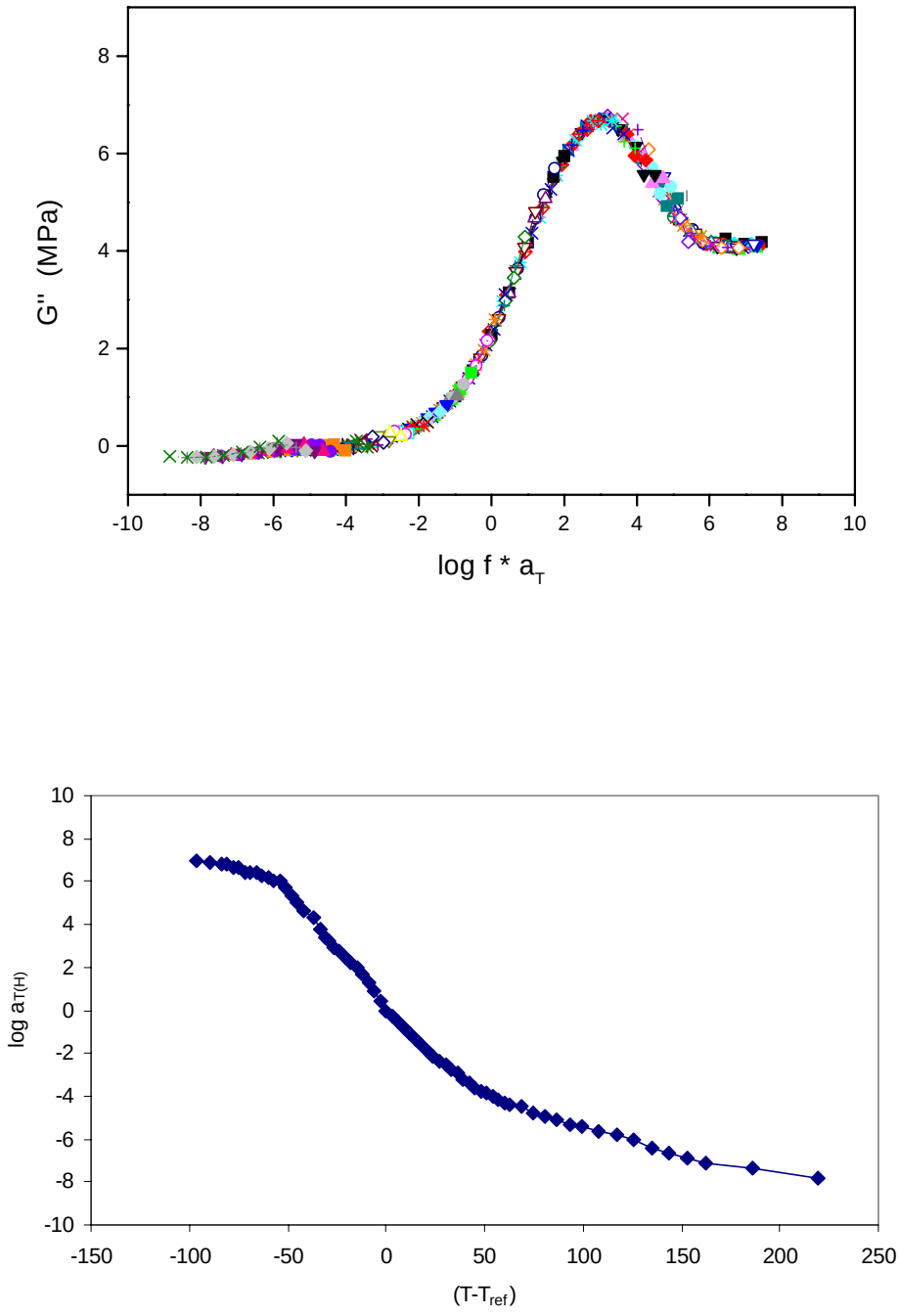

Figure 6-12. Frequency-temperature dynamic loss modulus master curve and the corresponding temperature shift-factor plot of adhesive exposed to *ethyl propionate* penetrant for 10^0 minutes. (legend same as in Figure 6-5)

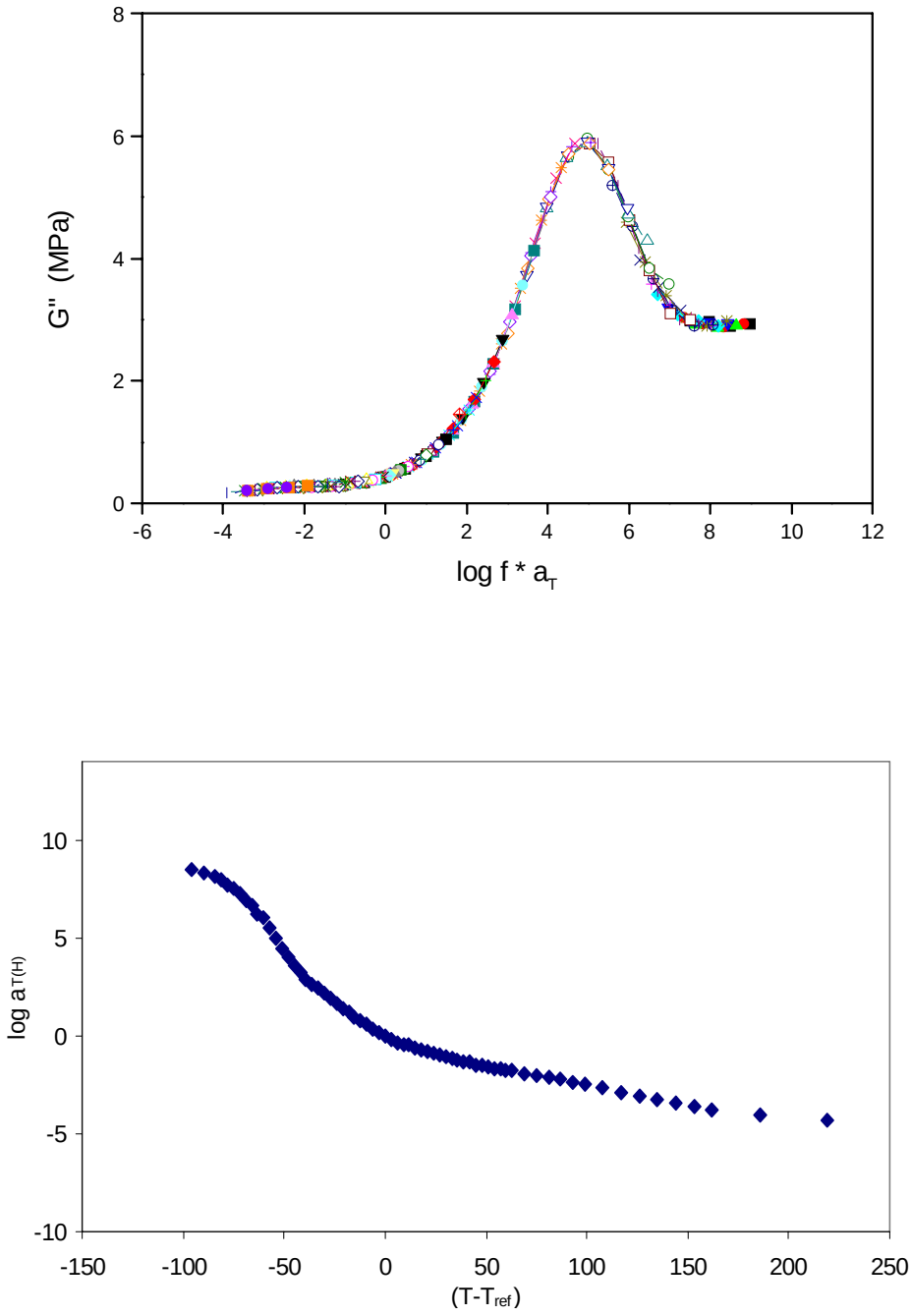

Figure 6-13. Frequency-temperature dynamic loss modulus master curve and the corresponding temperature shift-factor plot of adhesive exposed to *ethyl propionate* penetrant for 10^1 minutes. (legend same as in Figure 6-5)

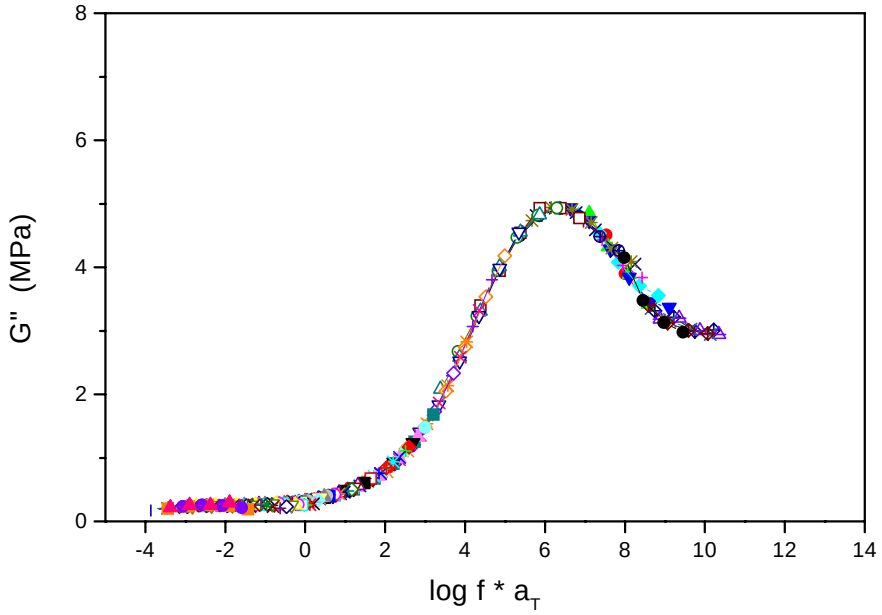

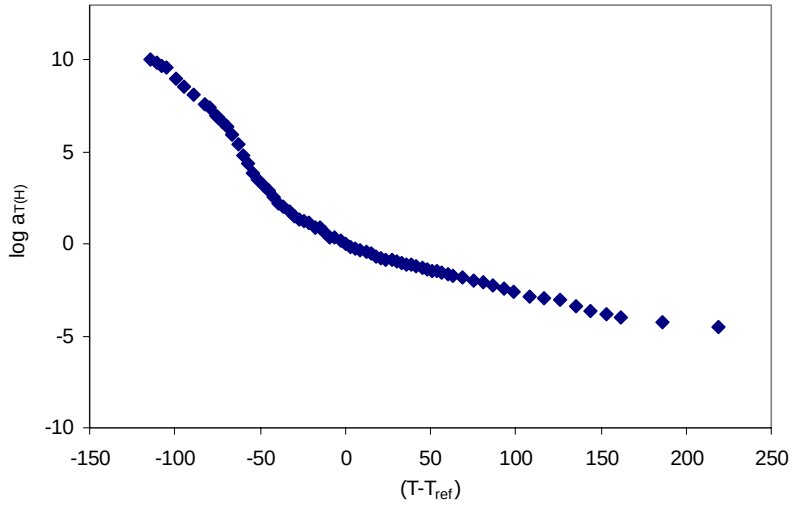

Figure 6-14. Frequency-temperature dynamic loss modulus master curve and the corresponding temperature shift-factor plot of adhesive exposed to *ethyl propionate* penetrant for $10^{3.70}$ minutes. (legend same as in Figure 6-5)

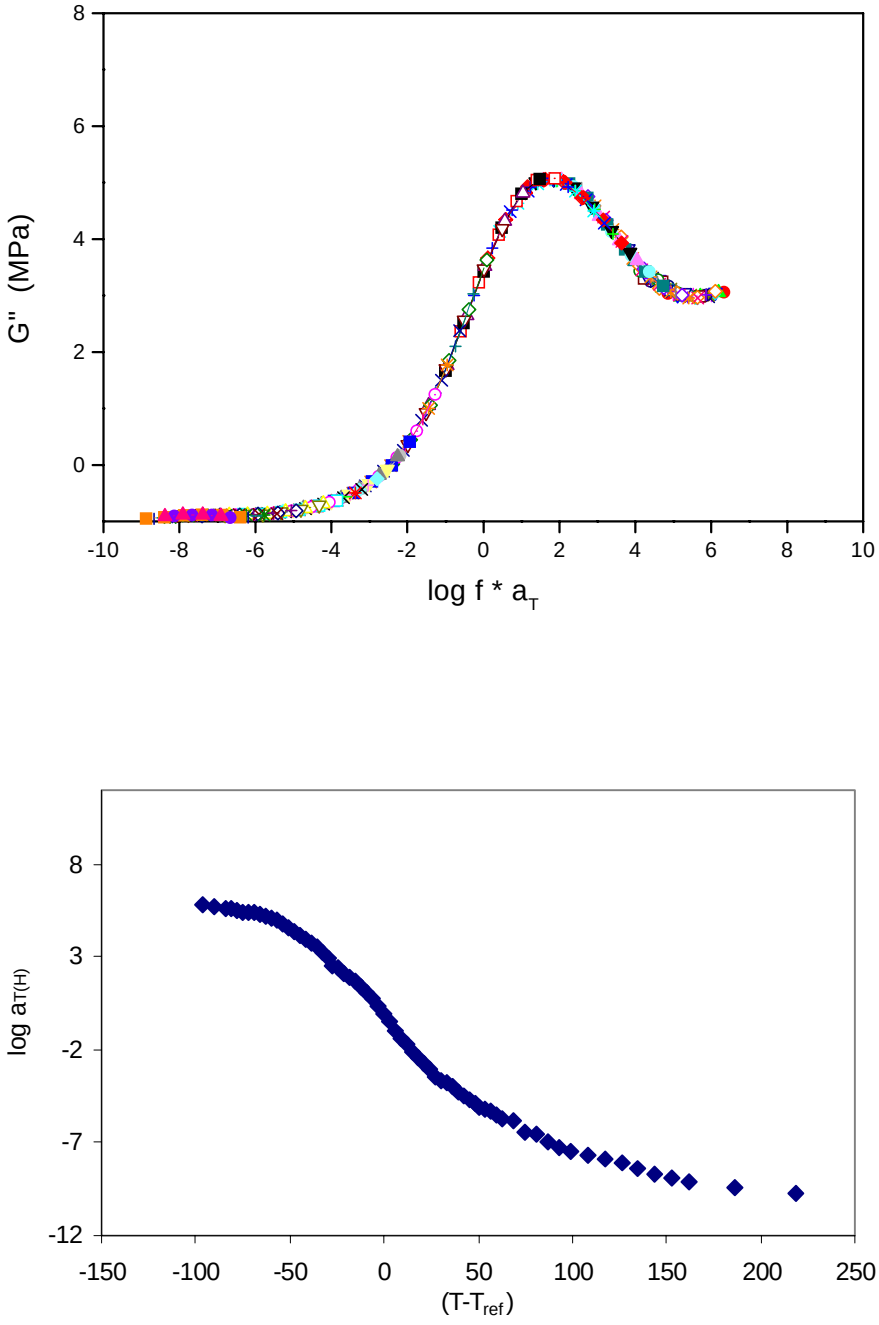

Figure 6-15. Frequency-temperature dynamic loss modulus master curve and the corresponding temperature shift-factor plot of adhesive exposed to *propyl butyrate* penetrant for 10^0 minutes. (legend same as in Figure 6-5)

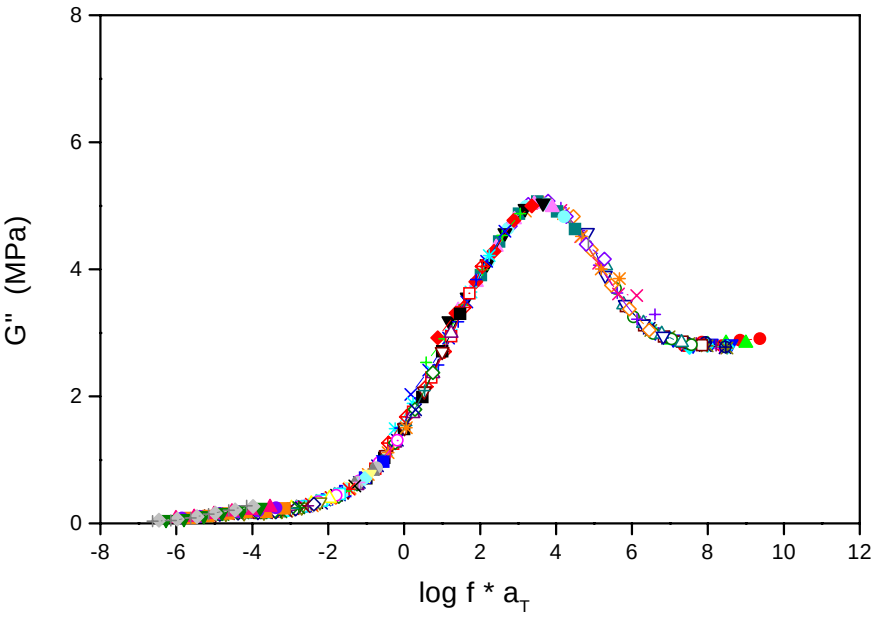

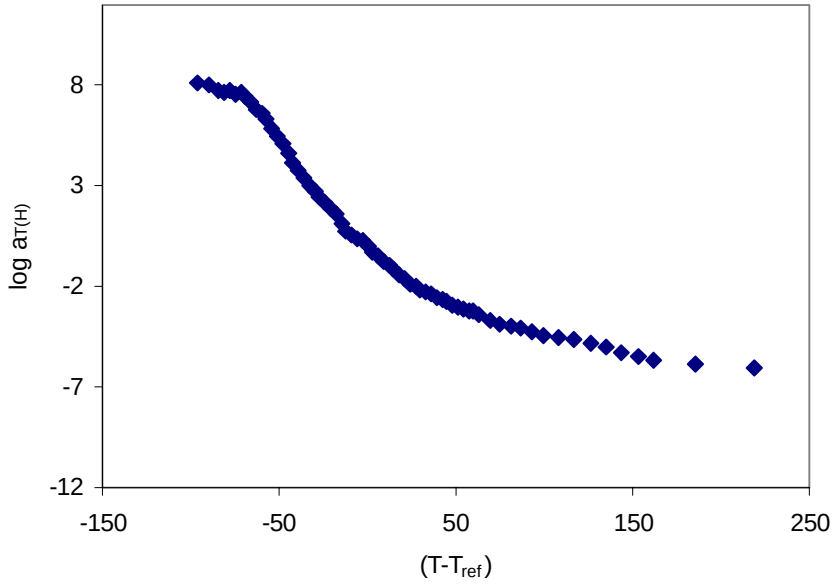

Figure 6-16. Frequency-temperature dynamic loss modulus master curve and the corresponding temperature shift-factor plot of adhesive exposed to *propyl butyrate* penetrant for 10^1 minutes. (legend same as in Figure 6-5)

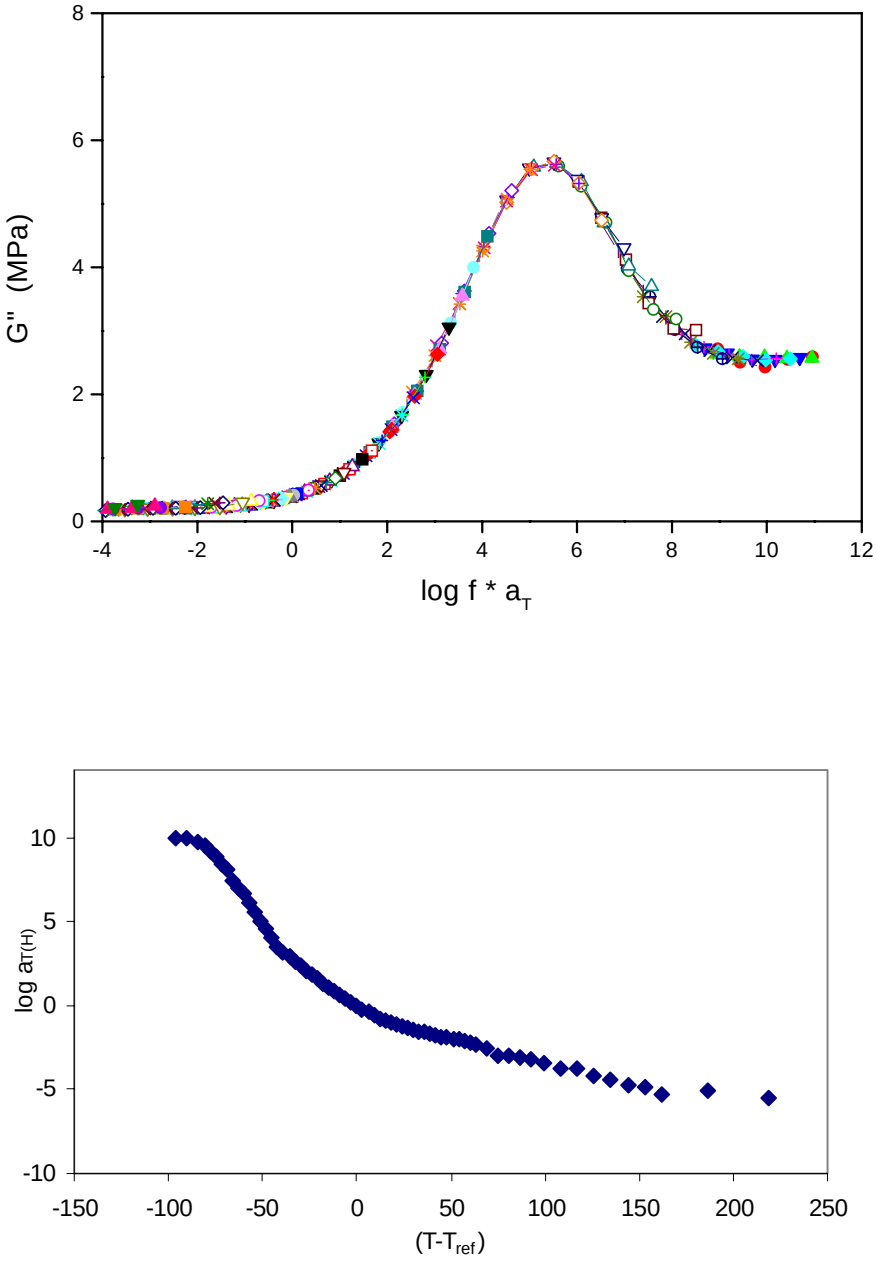

Figure 6-17. Frequency-temperature dynamic loss modulus master curve and the corresponding temperature shift-factor plot of adhesive exposed to *propyl butyrate* penetrant for 10^3 minutes. (legend same as in Figure 6-5)

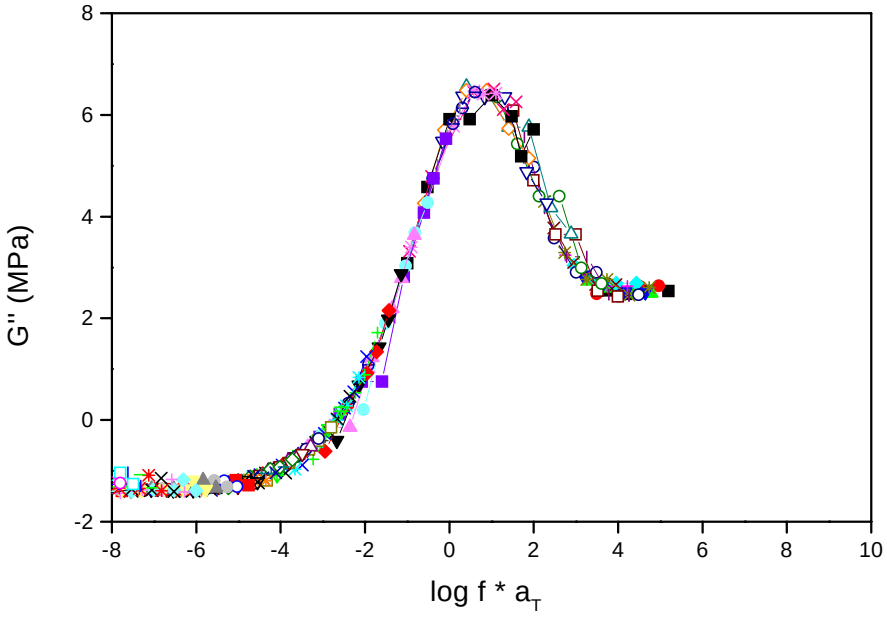

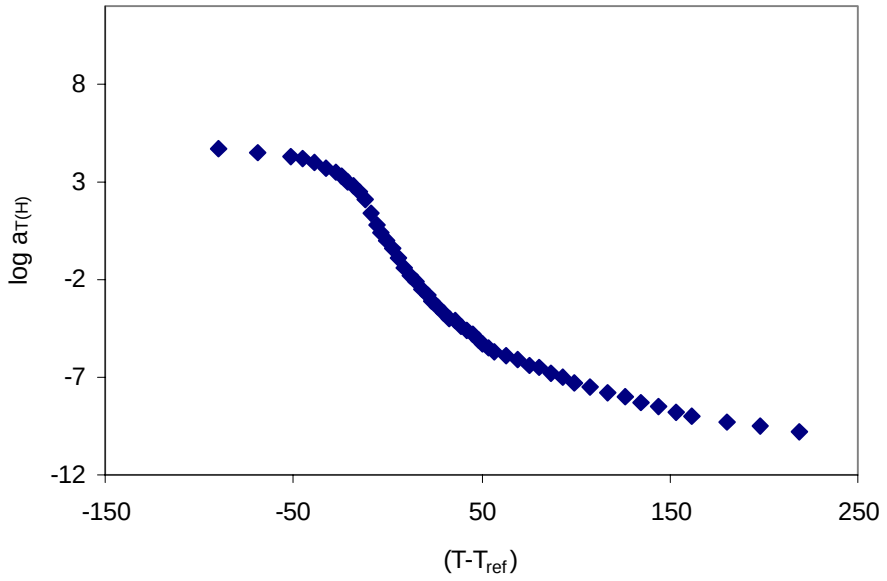

Figure 6-18. Frequency-temperature dynamic loss modulus master curve and the corresponding temperature shift-factor plot of adhesive exposed to *ethyl myristate* penetrant for 10^0 minutes. (legend same as in Figure 6-5)

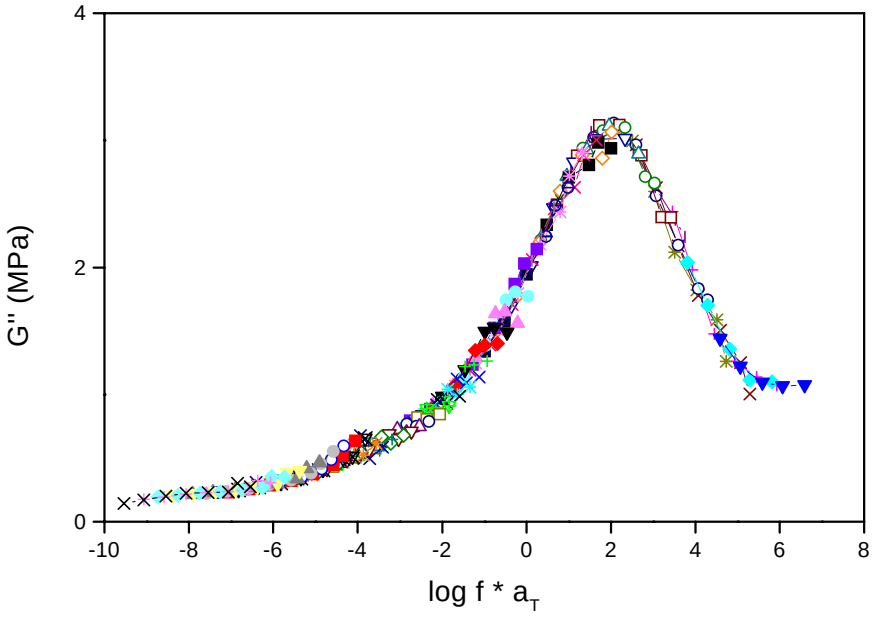

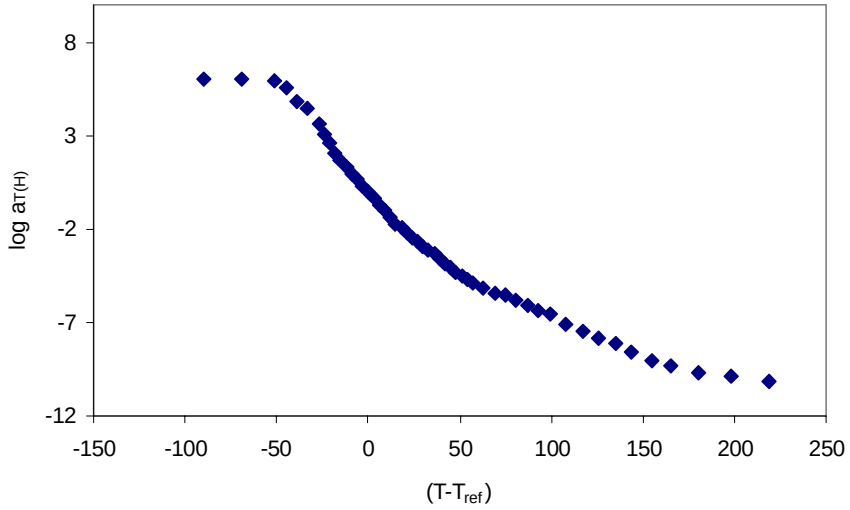

Figure 6-19. Frequency-temperature dynamic loss modulus master curve and the corresponding temperature shift-factor plot of adhesive exposed to *ethyl myristate* penetrant for 10^1 minutes. (legend same as in Figure 6-5)

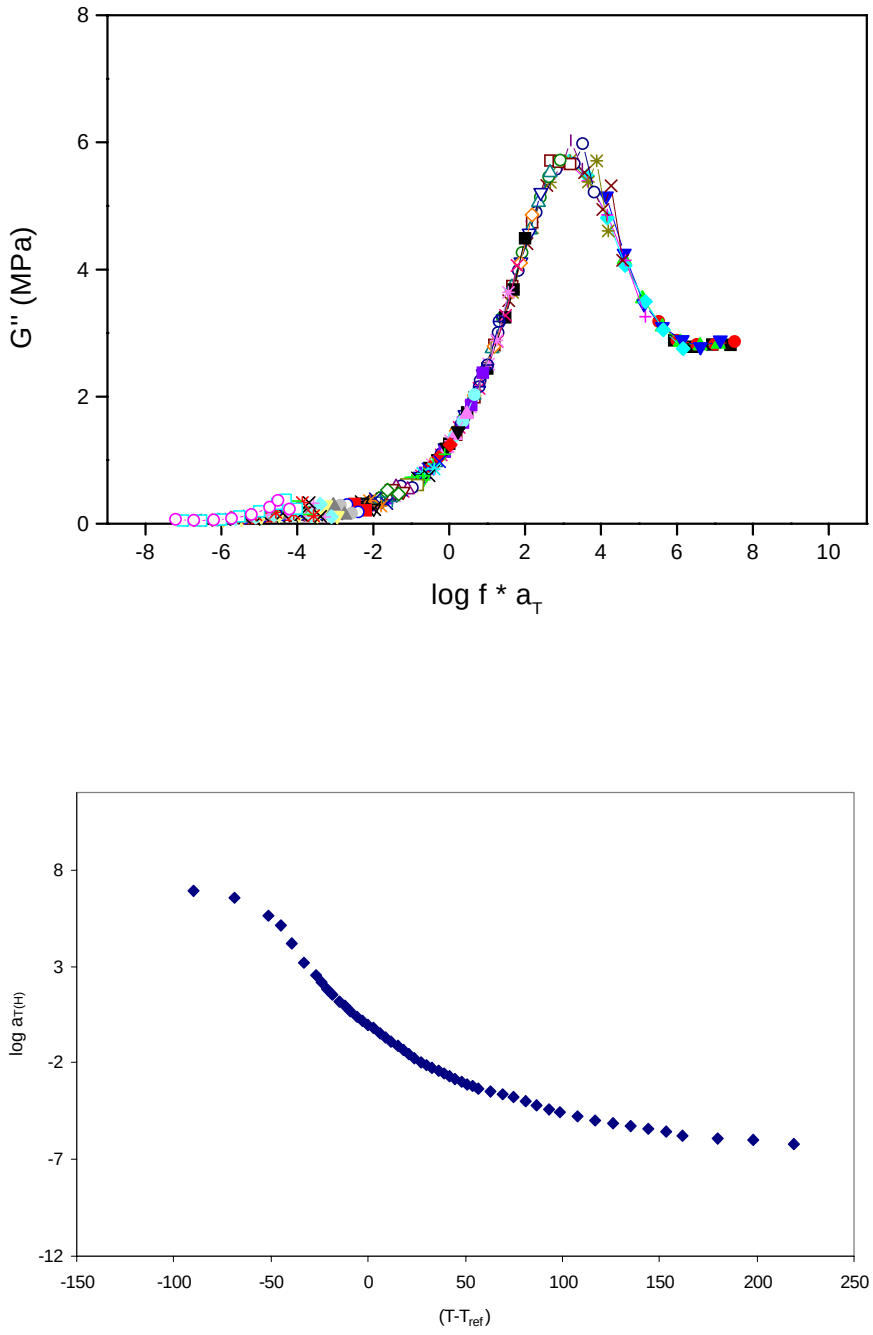

Figure 6-20. Frequency-temperature dynamic loss modulus master curve and the corresponding temperature shift-factor plot of adhesive exposed to *ethyl myristate* penetrant for $10^{3.70}$ minutes. (legend same as in Figure 6-5)

Table 6-1. C_1 and C_2 values evaluated from frequency-temperature master curves of adhesive exposed to hexane

Hexane		
Exposure time (min)	C_1	C_2
10^0	14.04	84.01
10^1	11.62	64.97
10^2	12.22	121.89
10^3	7.64	72.95
10^4	12.14	169.95

Table 6-2. C_1 and C_2 values evaluated from frequency-temperature master curves of adhesive exposed to heptane

Heptane		
Exposure time (min)	C_1	C_2
10^0	15.12	103.40
10^1	14.20	95.58
10^2	13.09	100.40
10^3	9.93	90.32
10^4	11.49	116.80
10^5	11.13	88.40

Table 6-3. C_1 and C_2 values evaluated from frequency-temperature master curves of adhesive exposed to nonane

Nonane		
Exposure time (min)	C_1	C_2
10^0	12.05	74.27
10^1	13.53	85.22
10^2	11.24	67.18
10^3	10.84	89.38
10^4	9.55	85.13
10^5	10.52	93.10

Table 6-4. C_1 and C_2 values evaluated from frequency-temperature master curves of adhesive exposed to decane

Decane		
Exposure time (min)	C_1	C_2
10^0	11.79	83.09
10^1	9.55	57.78
10^2	16.53	185.48
10^3	16.75	213.98
$10^{3.70}$	9.51	84.36
10^4	10.53	82.15
10^5	8.03	76.01

Table 6-5. C_1 and C_2 values evaluated from frequency-temperature master curves of adhesive exposed to undecane

Undecane		
Exposure time (min)	C_1	C_2
10^0	15.75	125.04
10^1	14.54	98.96
10^2	14.05	92.30
10^3	13.08	128.07
10^4	10.25	75.60
10^5	9.12	79.38

Table 6-6. C_1 and C_2 values evaluated from frequency-temperature master curves of adhesive exposed to tridecane

Tridecane		
Exposure time (min)	C_1	C_2
10^0	18.17	163.22
10^1	16.28	110.26
10^2	12.12	75.70
10^3	12.18	74.02
10^4	10.92	113.35
10^5	11.77	96.22

Table 6-7. C_1 and C_2 values evaluated from frequency-temperature master curves of adhesive exposed to pentadecane

Pentadecane		
Exposure time (min)	C_1	C_2
10^0	14.03	82.36
10^1	10.78	62.23
10^2	12.31	71.78
10^3	12.70	77.77
10^4	15.50	178.21
10^5	8.66	77.76

Table 6-8. C_1 and C_2 values evaluated from frequency-temperature master curves of adhesive exposed to hexadecane

Hexadecane		
Exposure time (min)	C_1	C_2
10^0	10.31	77.21
10^1	11.07	67.92
10^2	10.12	62.15
10^3	10.00	62.17
10^4	12.20	84.34
$10^{4.60}$	20.54	233.48
10^5	11.22	131.17

Table 6-9. C_1 and C_2 values evaluated from frequency-temperature master curves of adhesive exposed to heptadecane

Heptadecane		
Exposure time (min)	C_1	C_2
10^0	11.88	75.11
10^1	12.43	89.54
10^2	12.13	66.27
10^3	12.77	68.16
$10^{3.70}$	15.90	94.06
$10^{4.60}$	14.82	93.15
10^5	14.65	189.09

Table 6-10. C_1 and C_2 values evaluated from frequency-temperature master curves of adhesive exposed to methyl acetate

Methyl Acetate		
Exposure time (min)	C_1	C_2
10^0	13.93	91.23
10^1	9.64	148.28
10^2	9.06	258.03
10^3	3.90	158.13
$10^{3.70}$	4.44	90.69

Table 6-11. C_1 and C_2 values evaluated from frequency-temperature master curves of adhesive exposed to ethyl propionate

Ethyl Propionate		
Exposure time (min)	C_1	C_2
10^0	14.86	151.83
10^1	10.47	133.14
10^2	5.48	115.94
10^3	4.44	105.91
$10^{3.70}$	7.78	214.14

Table 6-12. C_1 and C_2 values evaluated from frequency-temperature master curves of adhesive exposed to propyl butyrate

Propyl Butyrate		
Exposure time (min)	C_1	C_2
10^0	12.62	74.54
10^1	9.24	103.70
10^2	14.83	218.35
10^3	6.07	89.40
$10^{3.70}$	6.99	90.25
$10^{4.60}$	7.69	117.53

Table 6-13. C_1 and C_2 values evaluated from frequency-temperature master curves of adhesive exposed to ethyl heptanoate

Ethyl Heptanoate		
Exposure time (min)	C_1	C_2
10^0	12.11	72.09
10^1	13.53	117.60
10^2	10.52	108.94
10^3	6.97	86.82
$10^{3.70}$	12.46	135.24
$10^{4.60}$	5.58	62.72

Table 6-14. C_1 and C_2 values evaluated from frequency-temperature master curves of adhesive exposed to ethyl nonanoate

Ethyl Nonanoate		
Exposure time (min)	C_1	C_2
10^0	13.84	84.49
10^1	11.59	59.32
10^2	17.56	171.40
10^3	26.55	286.94
$10^{3.70}$	11.67	149.15
$10^{4.60}$	9.04	79.02

Table 6-15. C_1 and C_2 values evaluated from frequency-temperature master curves of adhesive exposed to ethyl undecanoate

Ethyl Undecanoate		
Exposure time (min)	C_1	C_2
10^0	12.71	81.14
10^1	11.43	46.96
10^2	13.81	123.41
10^3	11.12	112.56
$10^{3.70}$	8.56	76.19
$10^{4.60}$	10.91	103.07

Table 6-16. C_1 and C_2 values evaluated from frequency-temperature master curves of adhesive exposed to ethyl myristate

Ethyl Myristate		
Exposure time (min)	C_1	C_2
10^0	13.01	76.24
10^1	15.73	128.63
10^2	13.98	180.96
10^3	13.53	110.39
$10^{3.70}$	10.89	132.14

Table 6-17. C_1 and C_2 values evaluated from frequency-temperature master curves of adhesive exposed to isopropyl myristate

Isopropyl Myristate		
Exposure time (min)	C_1	C_2
10^1	12.50	76.06
10^2	12.58	78.41
10^3	8.34	95.82
$10^{3.70}$	11.25	98.85
10^4	11.75	133.25

Table 6-18. C_1 and C_2 values evaluated from frequency-temperature master curves of adhesive exposed to isodecyl pelargonate

Isodecyl Pelargonate		
Exposure time (min)	C_1	C_2
10^0	13.52	82.98
10^1	16.95	177.77
10^2	11.97	84.26
10^3	20.55	289.78
$10^{3.70}$	15.92	172.02
$10^{4.60}$	8.42	81.28

6.5 Diffusion-Time Master Curves

In the previous sections, the concept of frequency-temperature superpositioning was discussed. This process has enabled the prediction of the material response over a huge range of frequency, at a given reference temperature. The assumption in constructing these master curves is that the *mechanism of relaxation for the polyamide adhesive remains unchanged*, and that temperature changes only lead *to changes in the rate of the relaxation.* ("thermorheologically simple"). The next step of this study, which will be discussed in this section, is the extension of this concept to the transport process in the adhesive. This is often very difficult due to the changing nature of the polymer with time, during such a kinetic process. This type of behavior is usually termed "thermorheologically complex" and has been discussed in detail in the text by Aklonis[5]. The possibility of this behavior is well considered and will be discussed in detail with respect to this work later in this discussion.

For ease of discussion, the effects of increased exposure time on the dynamic mechanical spectra, with respect to only <u>one</u> of the penetrants out of the 18 penetrants studied, will be discussed below. It can be seen from Figure 6-21 that an increase in exposure time to the penetrant, decane from 10^2 to 10^5 minutes, shifts the mechanical spectrum towards higher frequencies. Since higher frequencies are analogous to lower temperatures, this effect can be interpreted in terms of depression of the T_g, to lower temperatures due to plasticization by the penetrant. This is typically what is expected on the basis of free volume theories[37,38,39].

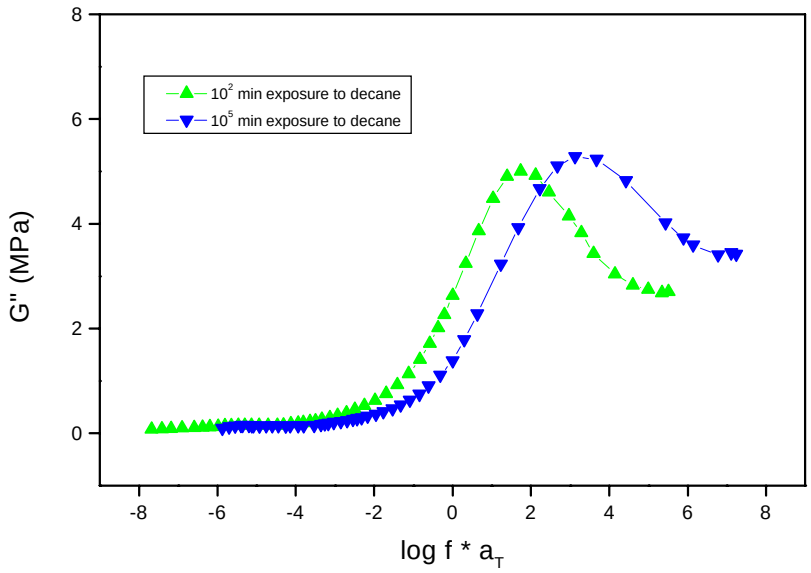

Figure 6-21. Frequency-temperature master curves for exposure times of 10^2 and 10^5 minutes to decane penetrant

The master curves for the two different exposure times shown in Figure 6-21, exhibit similar shapes, and appear as if they may be transposable. This introduces the concept of a potential shift factor based upon exposure time to a penetrant.

Using a method similar to McCrum, Read, and Williams[40], multiple curves were normalized with respect to their relaxed and unrelaxed moduli. The loss peaks were assumed to arise predominantly from the motions of the polymer itself. This is a valid assumption for the system studied, due to the fact that the penetrants used are poor solvents (high χ values), with relatively low solubilities. This assumption enabled the normalization by G''_{max}, thereby creating a common scale for comparison of the various experiments. This procedure has now become widely accepted, and is extensively used by several researchers. A good example is the study by Ishida et al.[41] on poly(vinyl acetate) and poly(vinyl benzoate), where this normalization has been utilized to create the master curves for the α-relaxation of these materials.

For a given solvent, each master curve representing a particular exposure time has been normalized to a common axis using the technique described above. These normalized master curves for the penetrant, decane are shown in Figure 6-22. The normalized master curves of a few other penetrants, representative of both the alkanes and the esters, are given in Figure 6-24 through Figure 6-29.

Then, all the curves have been shifted with respect to an exposure/diffusion time of 0 minutes, to achieve maximum overlap. The number of log(frequency) units by which each master curve was shifted is designated as a *diffusion-time shift factor*, $\log a_{Dt}$. The composite master-master curve, resulting from the translation of all the diffusion-time master curves for decane, shifted with respect to a reference time of 0 minutes, is also shown in Figure 6-22. The diffusion-time shift factors ($\log a_{Dt}$) calculated from Figure 6-22 are plotted as a function of log(exposure time) in Figure 6-23. The composite master-master curves corresponding to the previous examples are also shown in Figure 6-24 through Figure 6-29.

The diffusion-time shift factors, $\log a_{Dt}$, for the *n*-alkane and ester penetrant series, normalized with respect to their equilibrium diffusion times, t_e, are shown in Figure 6-30 and Figure 6-31, respectively. It can be seen from these figures that all of the 40 or more diffusion-time shift factors, within a penetrant series, can be represented by a single curve. This implies that the mechanism of polymer relaxation, for each penetrant series, is not altered by the presence of the penetrant.

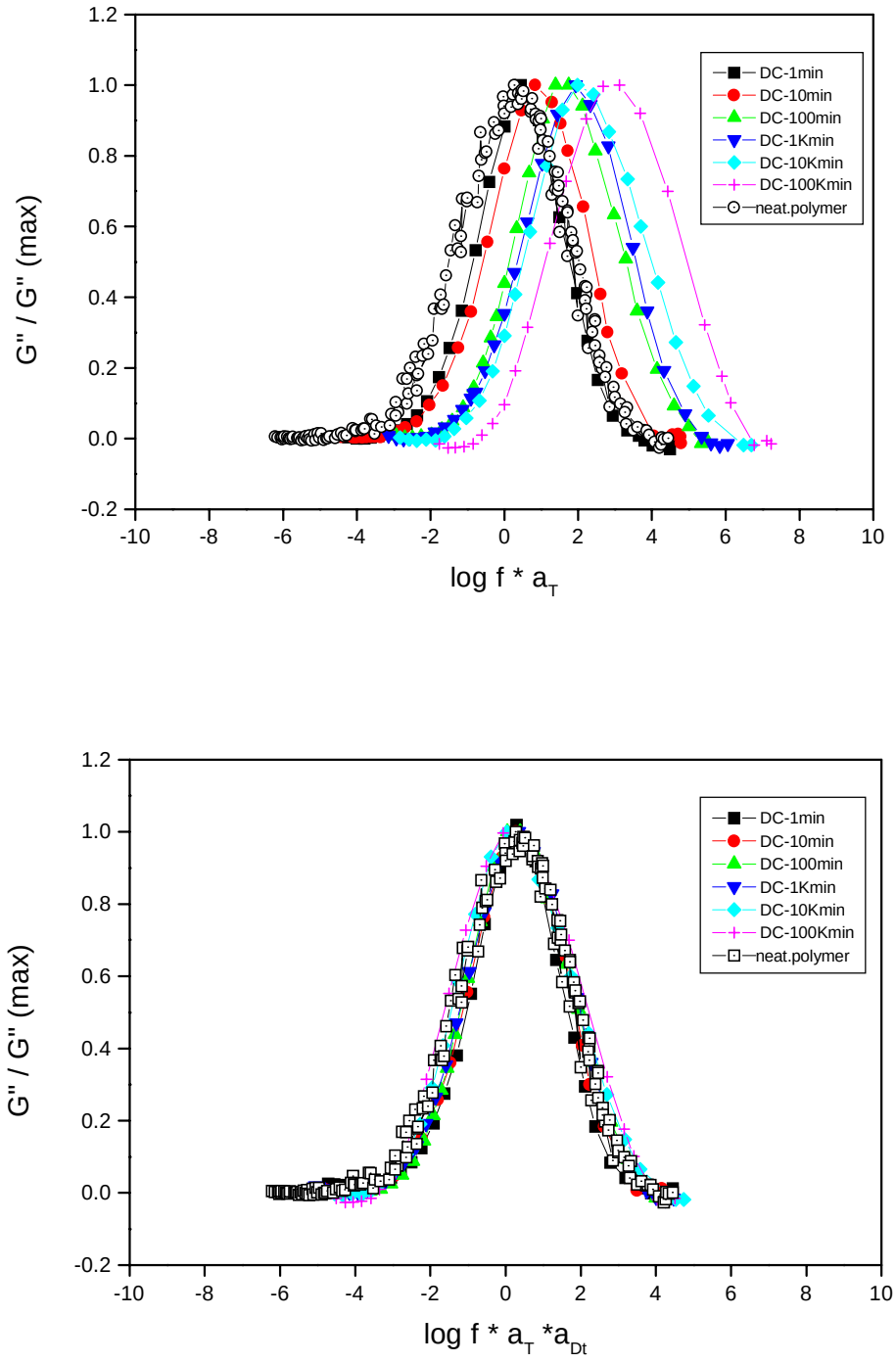

Figure 6-22. Normalized frequency-temperature master curves for various penetrant exposure times to *decane* (top). Doubly reduced temperature and diffusion-time master-master curves for penetrant, *decane* (bottom).

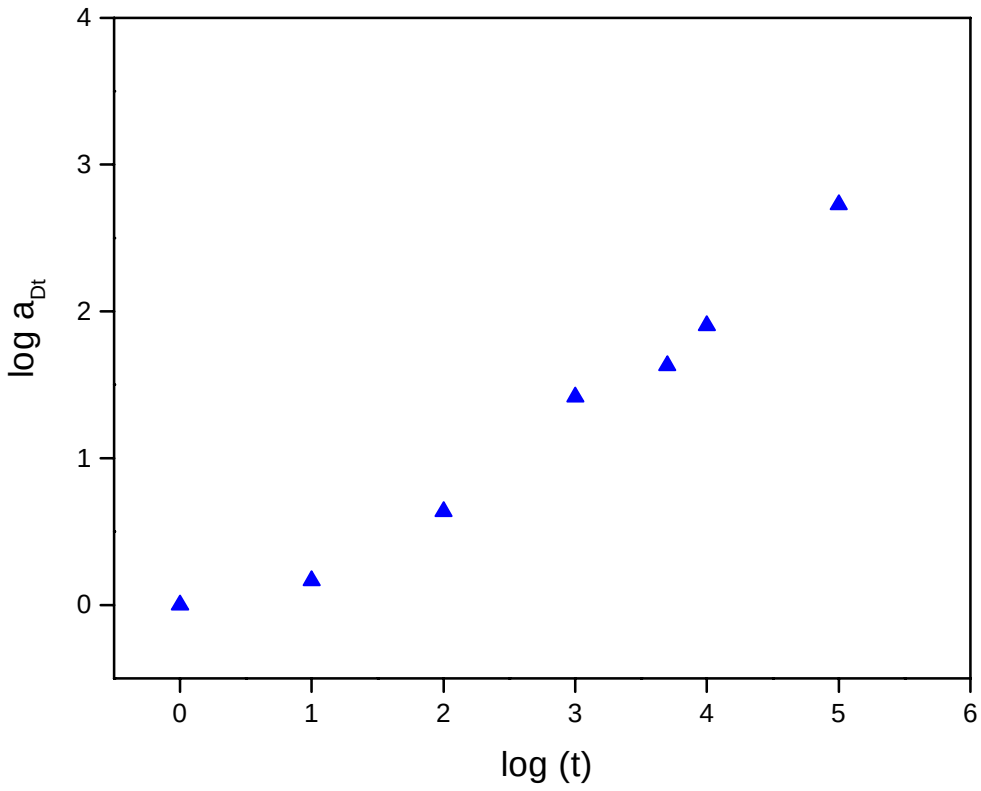

Figure 6-23. Diffusion-time shift factors, log a_{Dt}, for adhesive exposed to *decane* at various times.

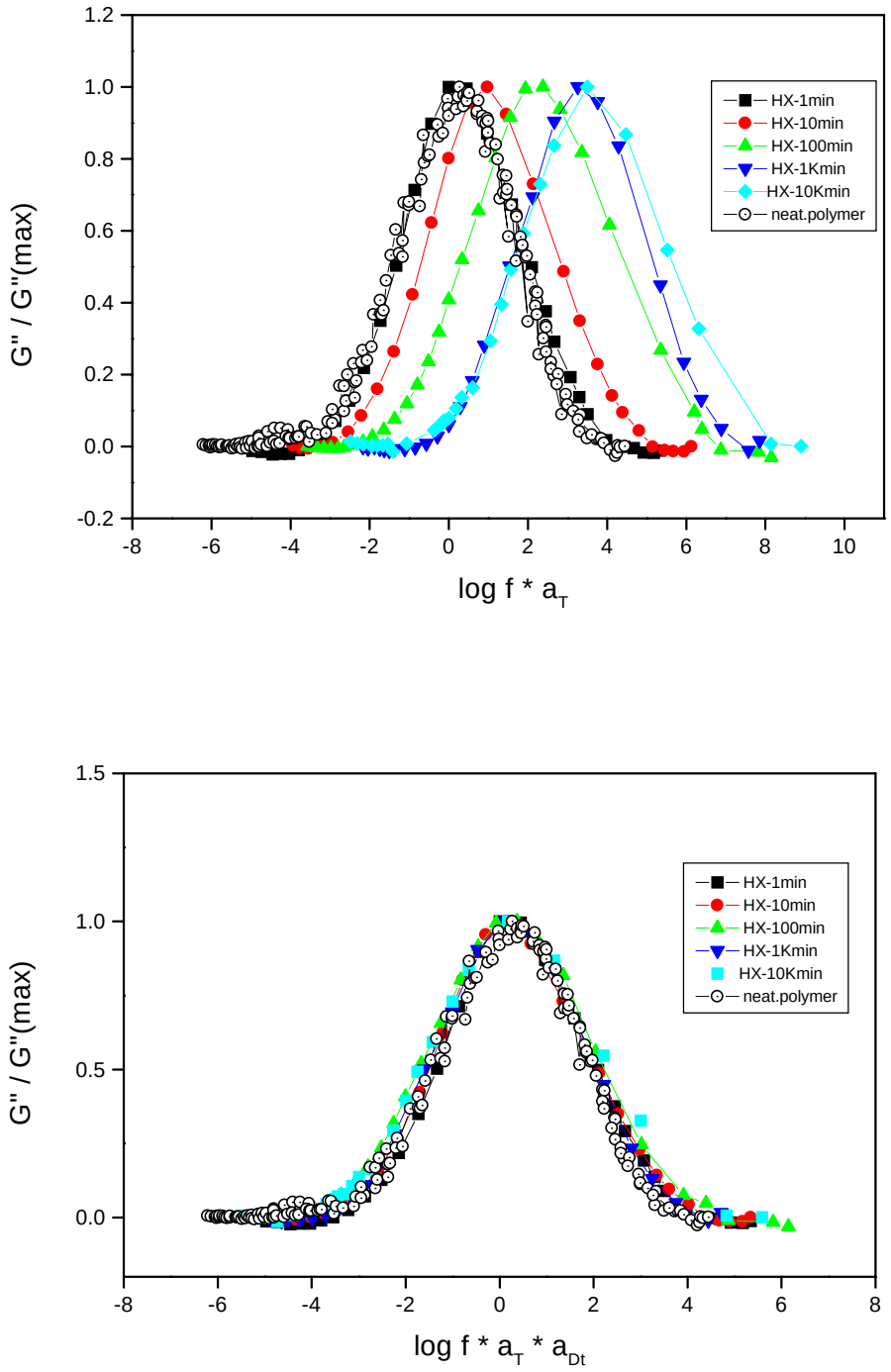

Figure 6-24. Normalized frequency-temperature master curves for various penetrant exposure times to *hexane* (top). Doubly reduced temperature and diffusion-time master-master curves for penetrant, *hexane* (bottom).

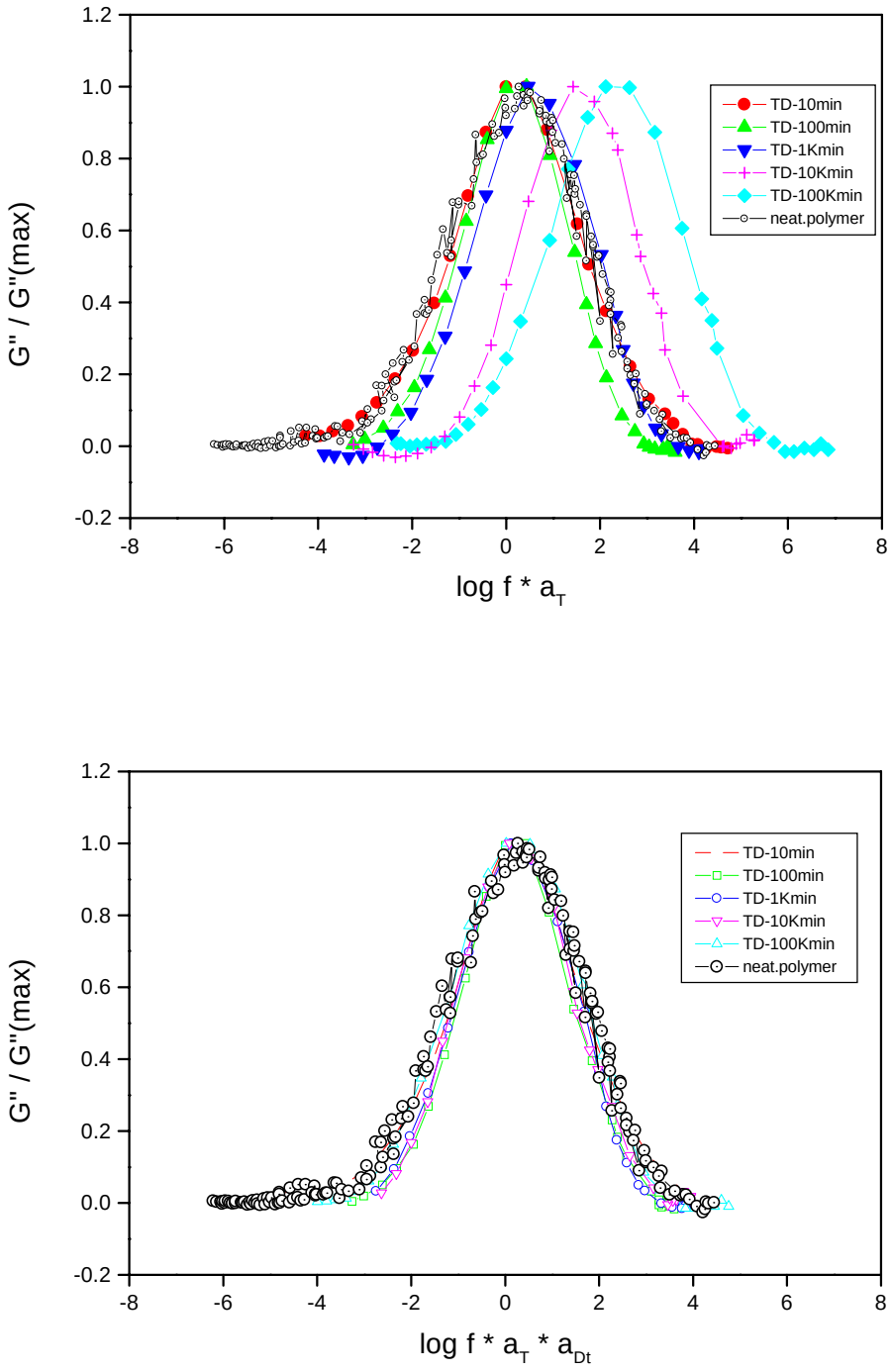

Figure 6-25. Normalized frequency-temperature master curves for various penetrant exposure times to *tridecane* (top). Doubly reduced temperature and diffusion-time master-master curves for penetrant, *tridecane* (bottom).

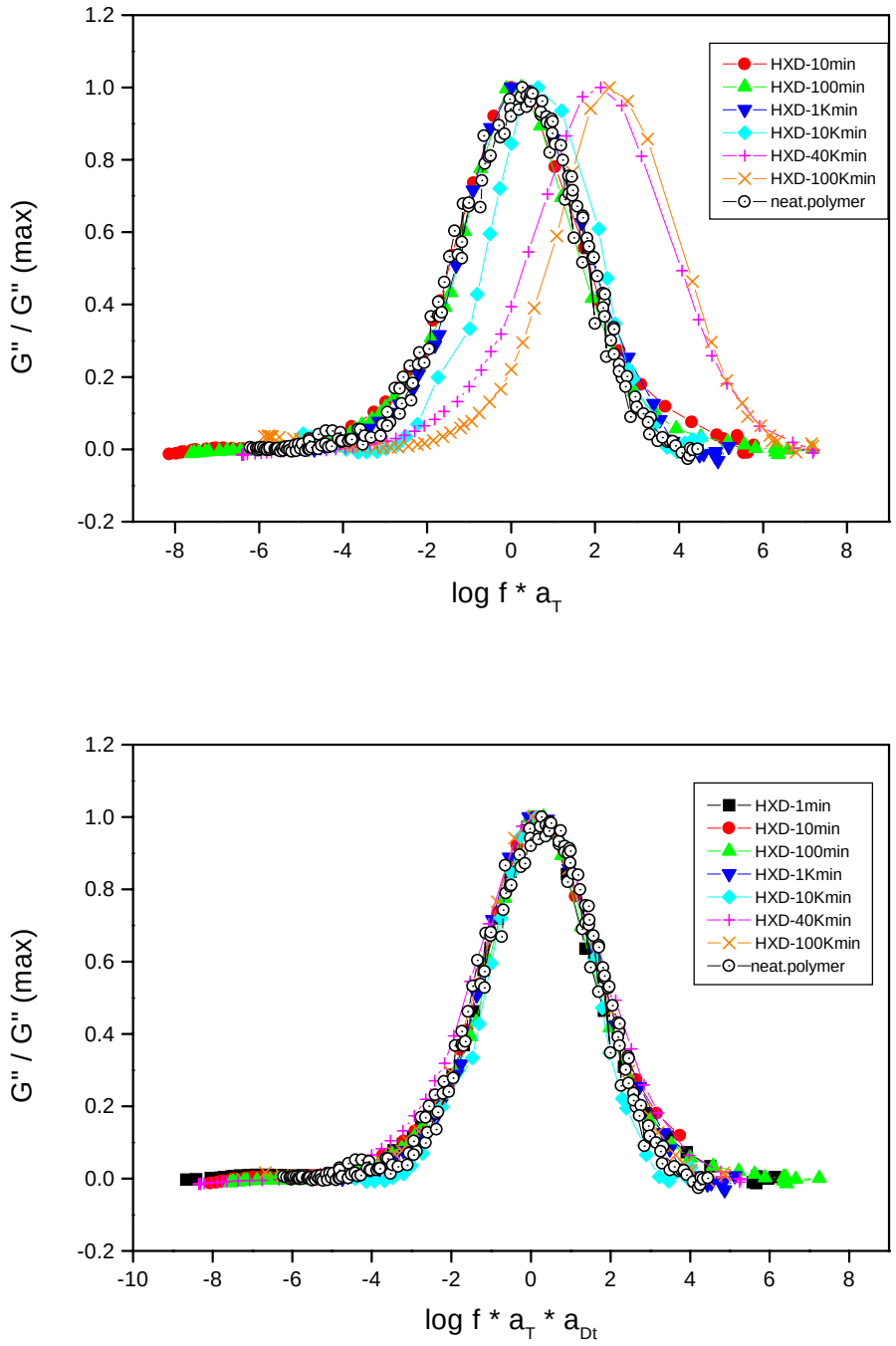

Figure 6-26. Normalized frequency-temperature master curves for various penetrant exposure times to *hexadecane* (top). Doubly reduced temperature and diffusion-time master-master curves for penetrant, *hexadecane* (bottom).

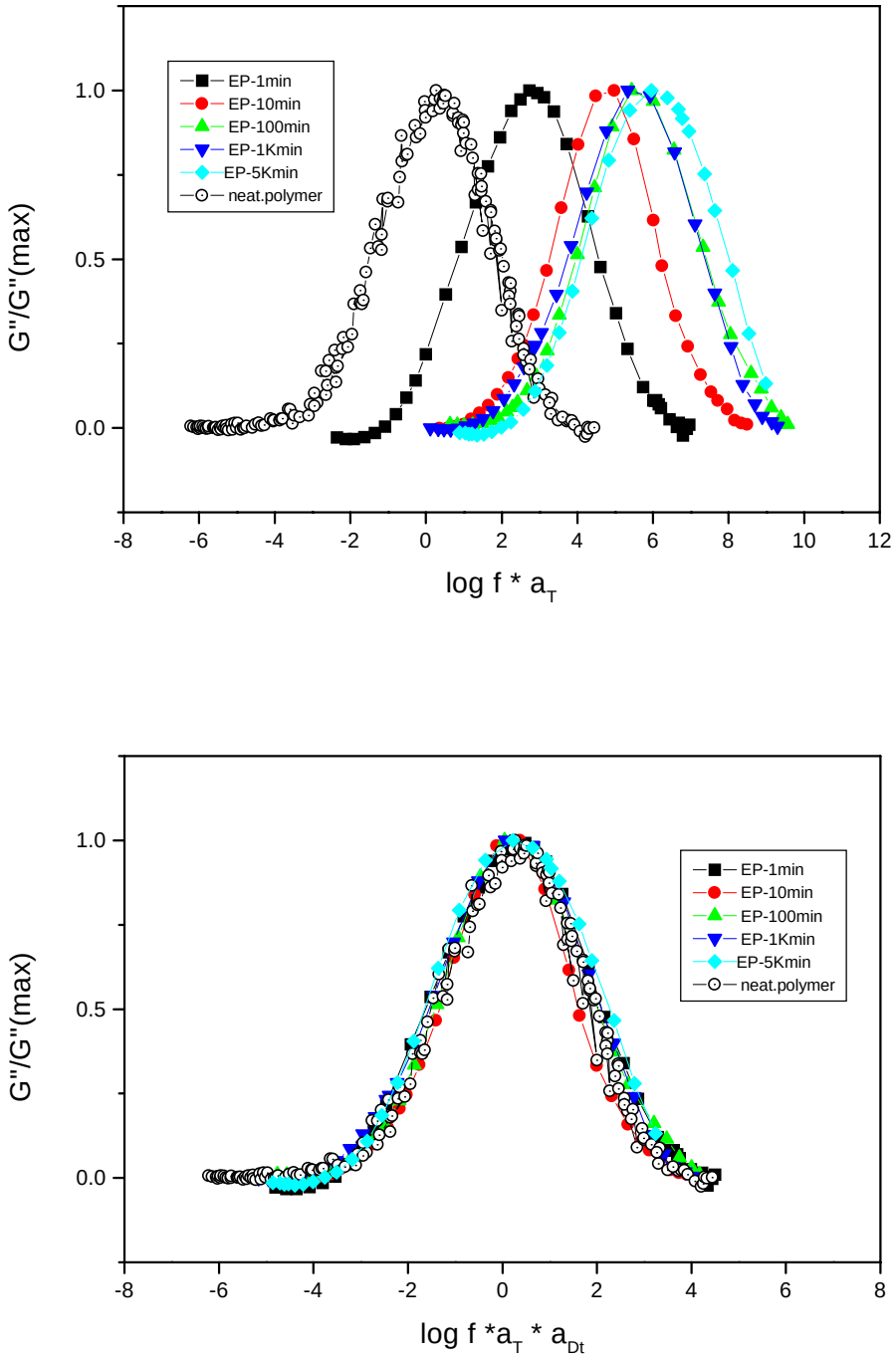

Figure 6-27. Normalized frequency-temperature master curves for various penetrant exposure times to *ethyl propionate* (top). Doubly reduced temperature and diffusion-time master-master curves for penetrant, *ethyl propionate* (bottom).

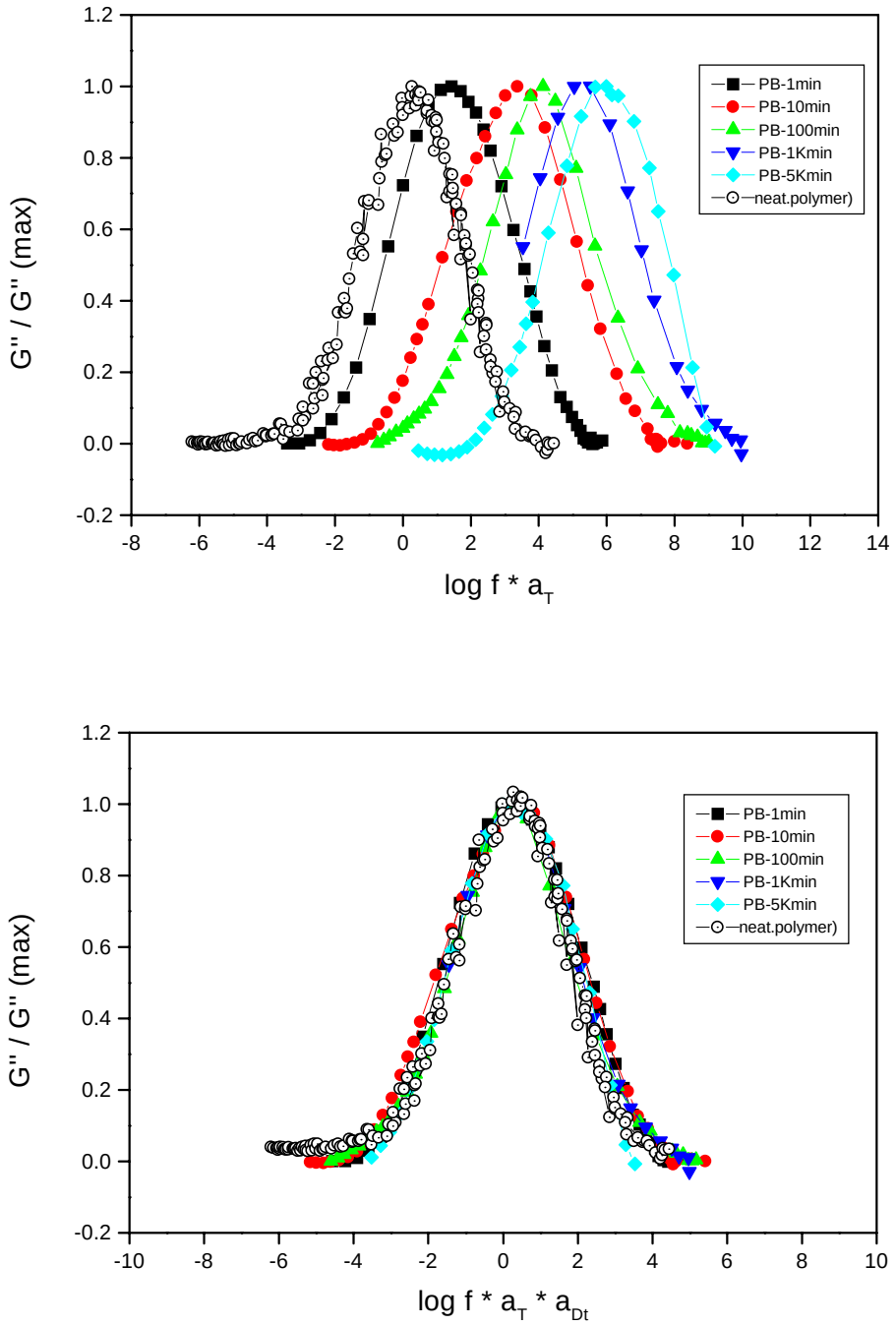

Figure 6-28. Normalized frequency-temperature master curves for various penetrant exposure times to *propyl butyrate* (top). Doubly reduced temperature and diffusion-time master-master curves for penetrant, *propyl butyrate* (bottom).

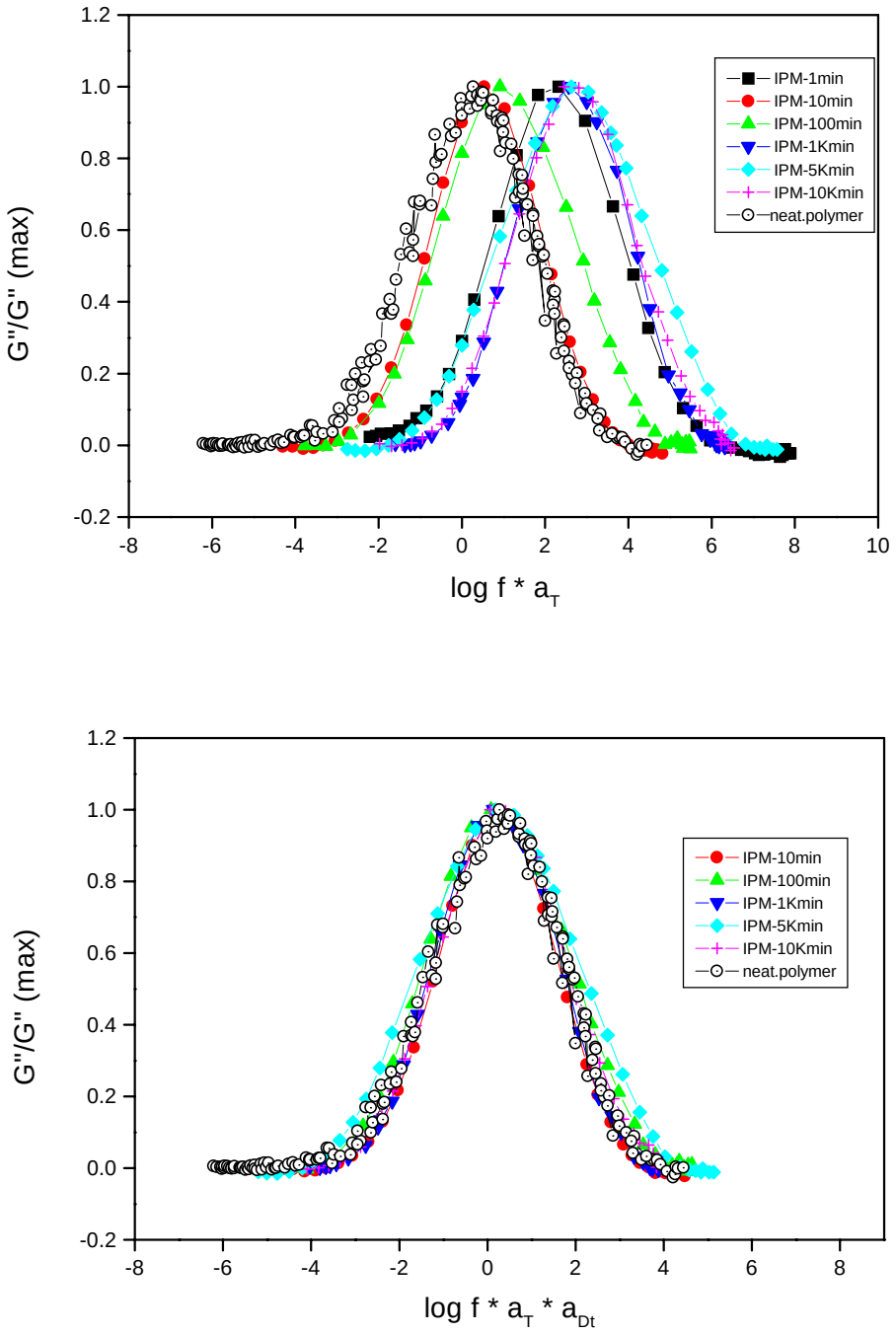

Figure 6-29. Normalized frequency-temperature master curves for various penetrant exposure times to *isopropyl myristate* (top). Doubly reduced temperature and diffusion-time master-master curves for penetrant, *isopropyl myristate* (bottom).

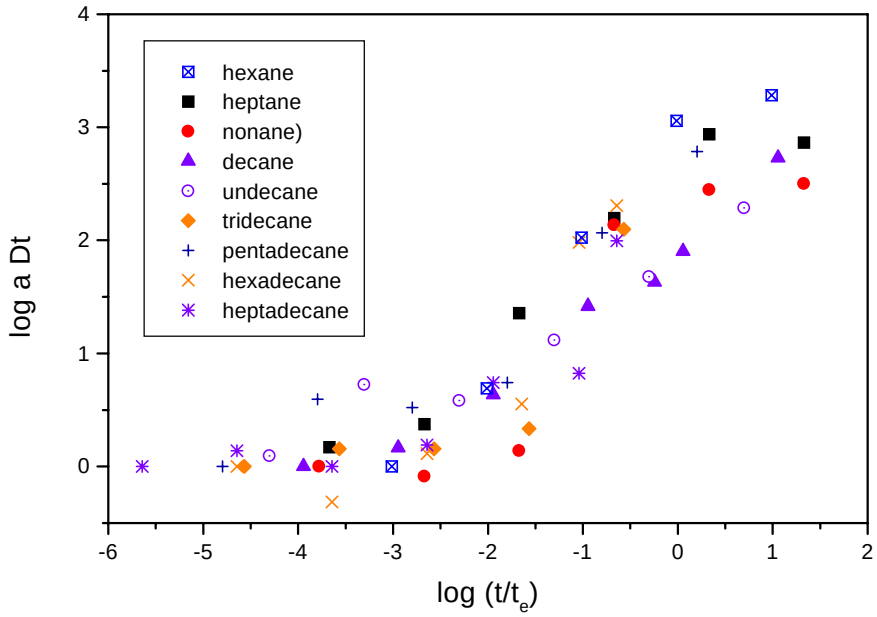

Figure 6-30. Diffusion-time shift factors for *n*-alkanes as a function of normalized time

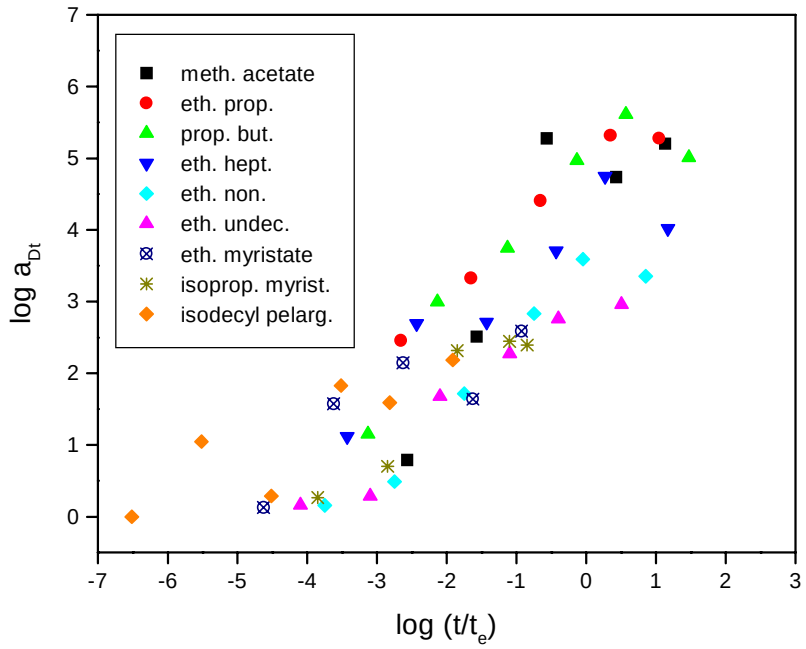

Figure 6-31. Diffusion-time shift factors for esters as a function of normalized time

This result is consistent with the principles of time-temperature superposition that have been invoked in the construction of the doubly reduced master curves. It also lends validity to the concept of a diffusion-time shift factor that has been introduced.

The shape of the curves in Figure 6-30 and Figure 6-31 closely resemble a sigmoidal statistical distribution. This resemblance observed is especially good, considering the difficult nature of the experiments. The sigmoidal shape could possibly be related to the fact that diffusion processes are often modeled as being a result of statistical jumps via Brownian motion[42].

It was mentioned earlier that the mechanism of polymer relaxation is not altered by the presence of the penetrant, while its rate is accelerated. The presence of the penetrant causes the film to swell, resulting in an increase in the free volume of the polymer matrix. The effect of this free volume increase is to accelerate the rate of relaxation of the polymer. This is analogous to the acceleration of the polymer relaxation by the temperature variable, in the WLF theory[43].

Comparing the diffusion-time shift factor plots of the *n*-alkanes and esters, Figure 6-30 and Figure 6-31, respectively, some major differences as a result of the ester functionality can be seen. The magnitude of the ester shift factors approaches a higher value than that of the corresponding alkanes due to the increased solubility and plasticizing efficiency of the esters. The slope of the "linear" portion for esters is also greater than that of the alkanes. This is, once again, due to the higher diffusion rates and increased plasticizing efficiency of the ester penetrants. The above two results can also be predicted based upon the results of the diffusion experiments that were discussed in the previous chapter. Those results showed that the diffusion coefficients and solubilities of the ester penetrants were larger than those of the corresponding *n*-alkanes.

A double reduction in variables such as the one proposed, allows for prediction of the dynamic mechanical response of the R/flex 410 adhesive system as a function of temperature and exposure time to any of the penetrants studied. However, the utility of this procedure lies in relating the diffusion-time shift factor to the fundamentals of the diffusion process, itself. Diffusion is a process in which the concentration of a penetrant in a polymer matrix increases as a function of time. By nature of this process, exposure time to a penetrant is related to its concentration via the diffusion coefficient. Therefore, the diffusion-time shift factors ($\log a_{Dt}$) of the alkanes and esters can also be described as a function of concentration (weight fraction), as shown in Figure 6-32 and Figure 6-33, respectively.

Thus, if the diffusion coefficient of either type of penetrant at a given temperature is known, its concentration-time profile may be generated for any geometry, by solving the appropriate boundary conditions for Fick's second law. Such a concentration-time profile enables the correlation of the composition of a penetrant at any given exposure time. This composition, in turn, can be used to evaluate the diffusion-time shift factor, $\log a_{Dt}$, of the penetrant, at that exposure time. Then, a knowledge of $\log a_{Dt}$, in

conjunction with the frequency-temperature shift factor, log a_T, can be used to construct the final master curve, accounting for the effects of both, temperature and diffusion.

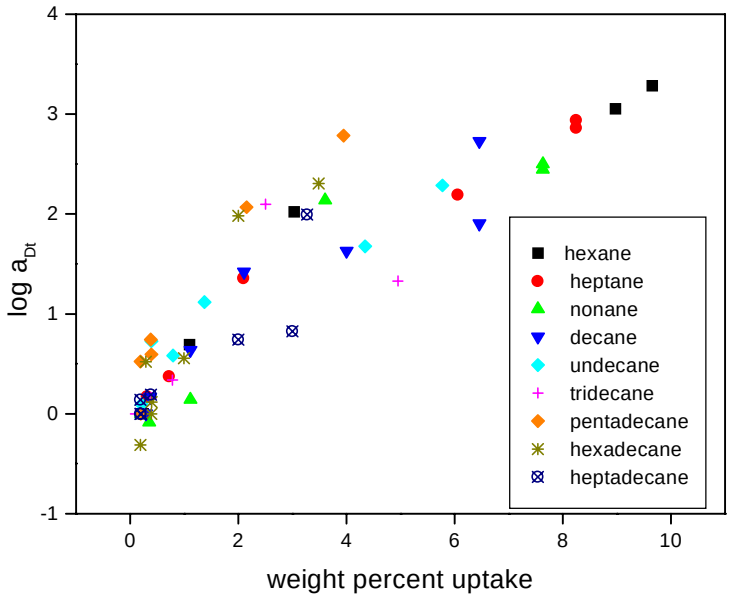

Figure 6-32. Diffusion-time shift factors as a function of penetrant composition for *n*-alkane penetrants

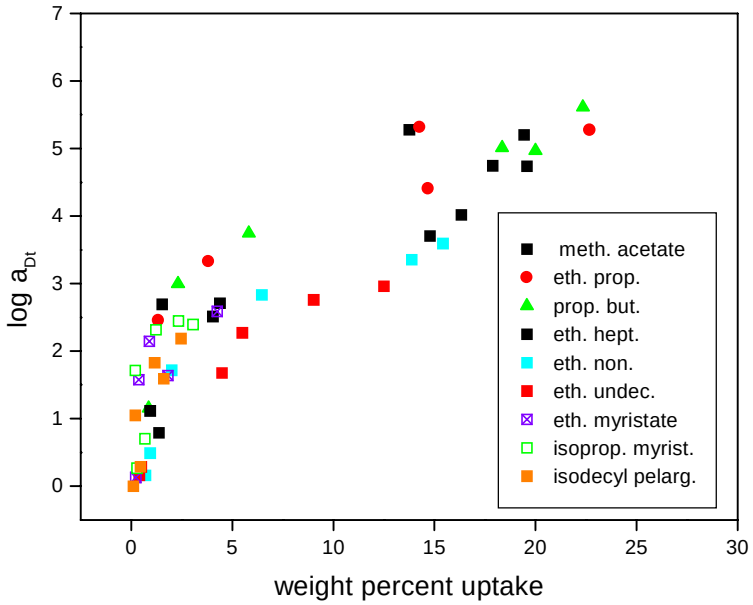

Figure 6-33. Diffusion-time shift factors as a function of penetrant composition for ester penetrants

6.6 Relaxation Behavior

6.6.1 Evaluation of H-N and KWW Parameters

In order to gain a deeper insight into the effects of the diffusion of the *n*-alkane and ester penetrants, the dynamic mechanical loss spectra were analyzed in greater detail. Segmental polymer relaxations occurring near the glass transition temperature typically involve localized motions of several backbone segments. Thus, the shape of the viscoelastic dispersion is expected to be reflective of local molecular structure[33]. Currently, only a few studies are known that have attempted to relate characteristics of the relaxation dispersion to chemical structure. In all of these studies changes in the chemical structure were induced by modifying the backbone of the polymer. However, in the current study, the backbone structure of the polymer investigated has been kept unchanged. Instead, the local environment of the polymer segments has been modified by the introduction of small molecular weight penetrants. Changes in the dispersion of the mechanical loss modulus spectra have been analyzed in terms of the β parameter from the KWW expression (Equ.(34)). The effects of penetrant absorption have also been investigated with respect to relaxation times and mean relaxation times of the polymer.

Using the procedure described in section 6.3, the dynamic loss moduli data of each frequency-temperature master curve, corresponding to a particular penetrant and exposure time has been fit to the Havriliak-Negami model of equation (26). The H-N model parameters have been calculated from those fits.

Using the Havriliak-Negami fitting parameters, the time-decaying function, $\Phi(t)$, (autocorrelation function) for each penetrant has also been evaluated. The autocorrelation functions, for the polymer at different exposure times to heptadecane (HPD) is shown as an example in Figure 6-34. These functions describe the relaxation process of the polymer as a function of time. The slopes of these functions are a measure of the relative rates of relaxation. With reference to the inflection point, it can be seen that the relaxation times become shorter as the penetrant exposure time increases. The autocorrelation function, $\Phi(t)$, of each polymer-penetrant system has been fit to the well-known Kohlrausch-Williams-Watts (KWW) time decay function (Equ.(34)) to yield the β parameter and τ_o, presently described as the KWW relaxation time. Quality of the fits was excellent with Chi^2 values ranging from 0.05 to 0.003. In addition, the gamma function described earlier (Equ. (37)) has been utilized to evaluate a mean relaxation time, $<\tau>$, for each system. These parameters will be discussed in more detail later.

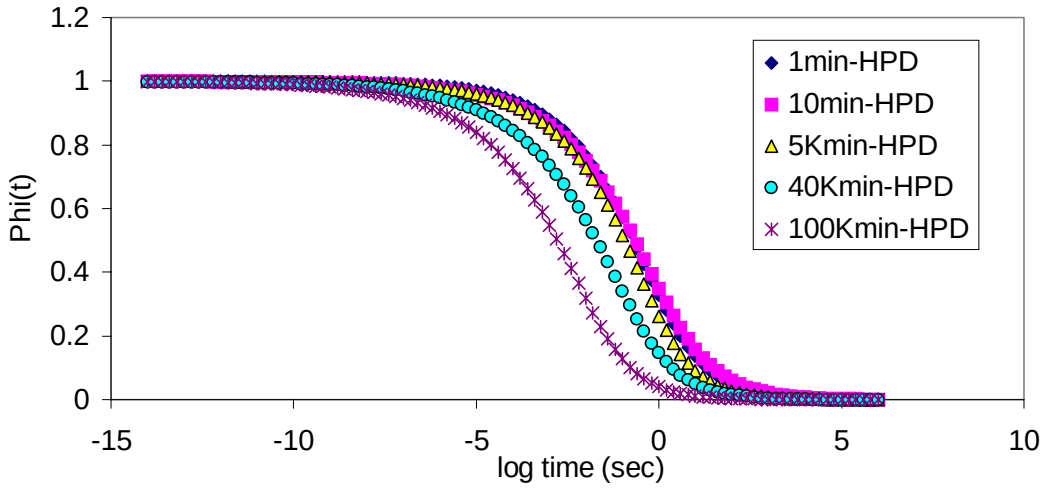

Figure 6-34. Autocorrelation decay functions, Φ(t), for polymer-penetrant system of heptadecane at various exposure times.

6.6.2 KWW Beta Parameter

The β-term in the KWW stretched-exponential characterizes the degree of non-exponentiality of the relaxation function. The KWW β-term has been physically interpreted by many researchers[30,31,44,45] as a description of the extent of molecular coupling within a polymer. Mathematically, the β-term is described as

$$\beta = 1 - n$$

where *n* is designated as a "coupling parameter." This coupling parameter, *n*, has been shown[46,33] to be proportional to the "strength of the constraints, or interactions with nonbonded neighboring segments" in the polymer. In this discussion, the KWW β-parameter will be used. However, its relationship to the coupling parameter, *n*, has been considered.

The experimental β values from the KWW non-linear fitting analysis for the *n*-alkanes are shown in Figure 6-35. There is a general decrease in the magnitude of β as exposure time to the alkane penetrants, increases. Due to the difficult nature of the experiments, the data shows some scatter. As a result, general linear trendlines have been drawn to aid in the comparison of the different penetrants. The order of magnitude (~0.2) of the evaluated beta parameters implies that the dispersion in relaxation distribution is very large. These small values of β result in large values for the coupling parameter, *n*, indicating that the polymer segmental relaxations require a high degree of cooperativity.

This interpretation is similar to that of a "fragile" material as described by Angell[47]. Similar values of n have been calculated for the highly cooperative systems such as poly(vinyl chloride)[44], Epon 1004 epoxy resin[44], and poly(vinyl methyl ether)-polystyrene blends[30]. The decrease in β observed in Figure 6-35 is a result of the greater variations of local molecular environments[45] of the polymer with time. As penetrant molecules become increasingly dispersed within the polymer sample, the distribution of penetrant molecules results in a spectrum of different local environments around individual polymer segments. Thus, the distribution of relaxation times can increase, regardless of whether or not the relaxation mechanism is the same.

As the size of the alkane penetrant decreases, the magnitude of β also decreases. The larger decrease in β for the smaller molecular weight penetrants is attributed to the higher degree of solubility of the smaller molecular weight penetrants. This, in turn, results in a higher composition of the penetrant, which further disperses itself amongst the different polymer segments creating a broader array of relaxing units. The larger molecular weight penetrants exhibit very little statistical change from the typical values of $\beta \approx 0.27$ for the neat polymer adhesive. From the above discussion, it can be seen that although the values of β exhibit a slight decrease with increasing exposure time and decreasing penetrant size, this decrease is *not* very significant (0.30 – 0.14). Therefore, the possibility that a change in relaxation mechanism could occur during the diffusion process is highly unlikely.

In the following paragraph, the KWW β-parameters obtained from the curve fitting of the ester penetrants will be discussed. Figure 6-36 shows a plot of β as a function of log (exposure time) for the ester series. For the larger molecular weight esters, the values of β decrease with increasing exposure time, as was observed with the *n*-alkanes. However, as the ester penetrants become more soluble, the values of β increase with exposure time which can be interpreted as a decrease in cooperativity.

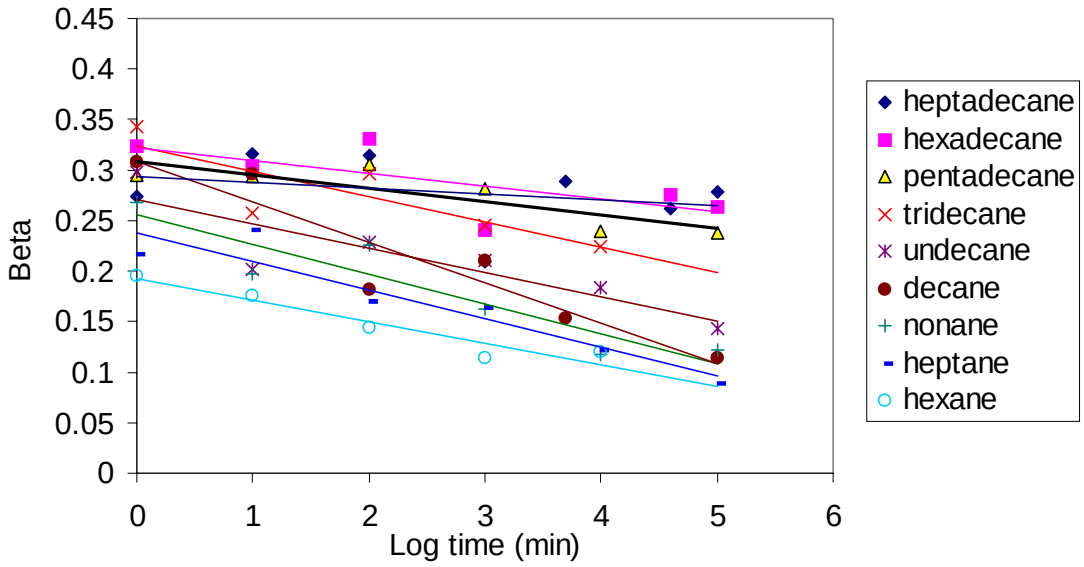

Figure 6-35. KWW Beta parameter as a function of exposure time to *n*-alkane penetrants

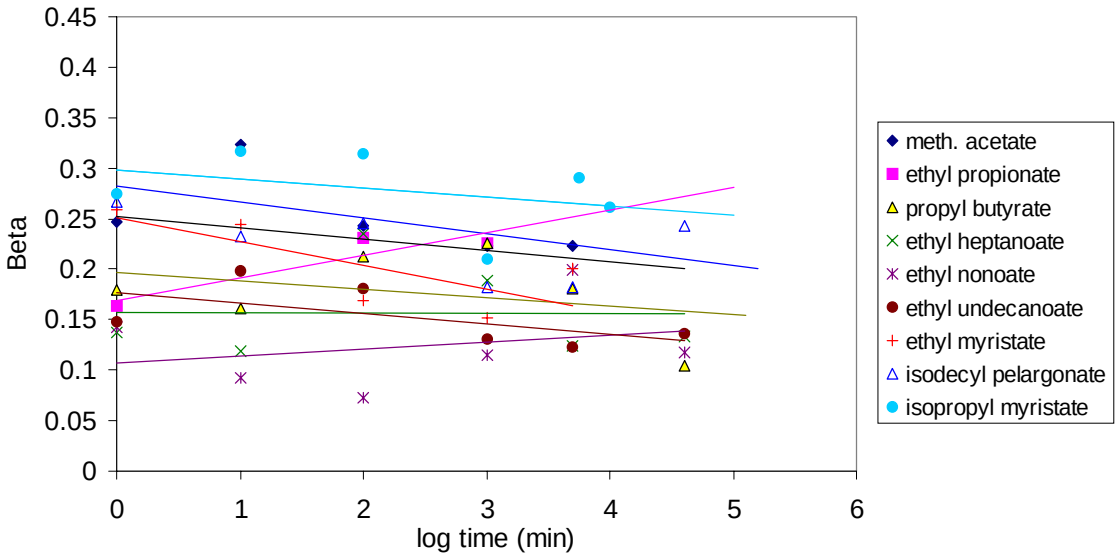

Figure 6-36. KWW Beta parameter as a function of exposure time to ester penetrants

The fact that the slopes of the lines become increasingly positive for the most soluble penetrants might be due to the fact that the higher degree of polarity results in a much higher degree of solubility. The increase in polarity promotes better distribution of the smaller ester penetrants since the polymer-penetrant interactions are greater. Furthermore, due to the higher levels of penetrant concentration, the differences in solvent concentration between different areas of the polymer matrix are relatively less. Both of the above effects lead to an increase in uniformity of penetrant distribution. As a result, the distribution of relaxation times becomes narrower, as the polymer segments now relax as similar cooperative units due to the greater uniformity in penetrant distribution.

As with the *n*-alkanes, the fact that the magnitudes of the β values do not change significantly for the esters, further supports the assumption that the polymer relaxation mechanism is not changing as a result of the transport process. This assumption will be further supported by the behavior of the relaxation times for each polymer-penetrant system.

It is implicit in the coupling model of molecular relaxation[30,4648] that time-temperature superpositioning is not valid for a system in which the β-parameter varies significantly. The root of this implication lies in the fact that changes in the relaxation distribution are often associated with changes in the relaxation mechanism. However, the β-parameter itself, has been shown to be highly sensitive to temperature[49], proving that it is not *always* constant for a given system, even though the relaxation mechanism remains unchanged.

The changes in β observed in the current study are relatively small, as described previously. They are believed to result not from any changes in the relaxation mechanism, but from changes in the time frames in which they occur throughout the polymer matrix. Furthermore, this study is not a strict assessment of either the principles of time-temperature superpositioning (tTSP) or of the coupling model for relaxation. Thus, the use of tTSP as an empirical method in the current study is valid and justified

6.6.3 Molecular Relaxation Times

In the previous section, the KWW β-parameter was discussed in detail, with particular attention to the coupling model of relaxation. A second KWW parameter designated as the $\tau_{o,}$ also results from the nonlinear fitting procedure. The KWW τ_o was described earlier as the time at which the time decaying function (TDF) decays to (1/e) of its original value. It is also designated as the *apparent* relaxation time. In the following section, this parameter, τ_o, and the concept of a *mean relaxation time*, $<\tau>$, will be discussed.

The KWW τ_o and the mean relaxation time, $<\tau>$, for the *n*-alkane series, are plotted as a function of normalized time, log (t/t_{eq}), in Figure 6-37 and Figure 6-38. The corresponding plots for the ester series are shown in Figure 6-39 and Figure 6-40. The behavior of the KWW relaxation time, $\tau_{o,}$ and that of the mean relaxation time, $<\tau>$, converge towards a single curve for all members of the *n*-alkane series. It may be recalled that this is very similar in shape and behavior to the diffusion-time shift factors (log a_{Dt}) plotted versus normalized time (log t/t_e). This behavior indicates that each alkane penetrant affects the relaxation times of the polymer in a similar manner.

As for the *n*-alkanes, the exponential decay in relaxation times for the ester penetrants is shown in Figure 6-39 and Figure 6-40. As in the *n*-alkane series, all the ester penetrants converge towards a single function. The normalized curves of Figure 6-39 and Figure 6-40 for the esters also follow the behavior of the normalized diffusion-time shift factor (log a_{Dt}) plots described earlier in section 6.4. The relaxation times at equilibrium for the *n*-alkanes and esters differ approximately by a factor of 2. This is the same difference that is observed between the diffusion-time shift factors at equilibrium for the esters and *n*-alkanes. This is expected since the diffusion of the penetrants alters the relaxation time of the polymer segments, which is manifested as a variation in the dynamic mechanical response of the polymer.

The fact that the relaxation times for both the ester and alkane series each converge towards single functions fortifies the idea that the mechanism of relaxation remains unchanged throughout the transport processes. The relaxation time analysis discussed above has enabled the evaluation of the parameters, τ_o and $<\tau>$, that possess physical significance. These parameters permit direct comparison of the effects of various penetrants as a function of exposure time. They have also provided a clearer picture of the effects of the transport process on the relaxation of the polymer. Furthermore, the behavior of the relaxation times and the discussion of the KWW β-term lend further support to the concept of the double reduction in temperature and diffusion time (log a_{Dt}) proposed earlier (section 6.4).

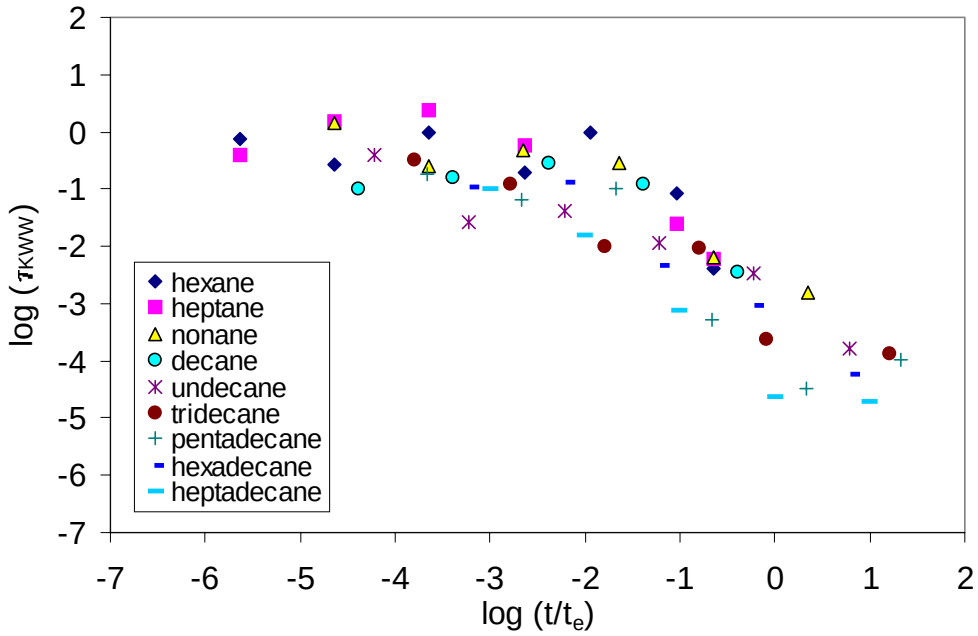

Figure 6-37. Evaluated KWW tau as a function of normalized time for polymer adhesive exposed to *n*-alkane penetrants.

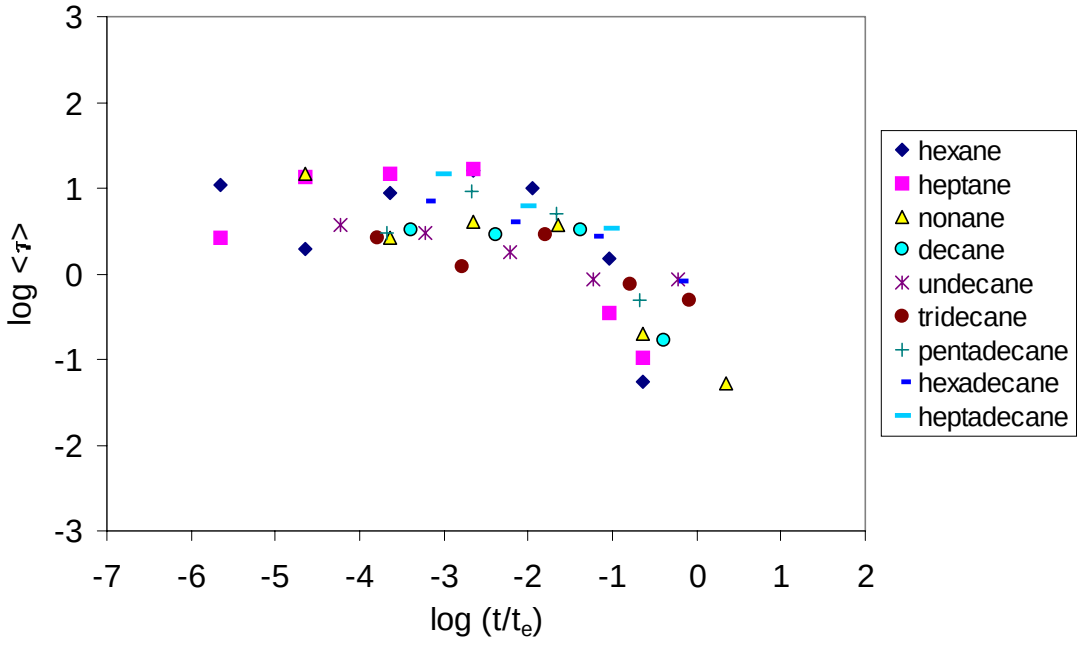

Figure 6-38. Evaluated mean relaxation time, < tau>, as a function of normalized time for polymer adhesive exposed to *n*-alkane penetrants.

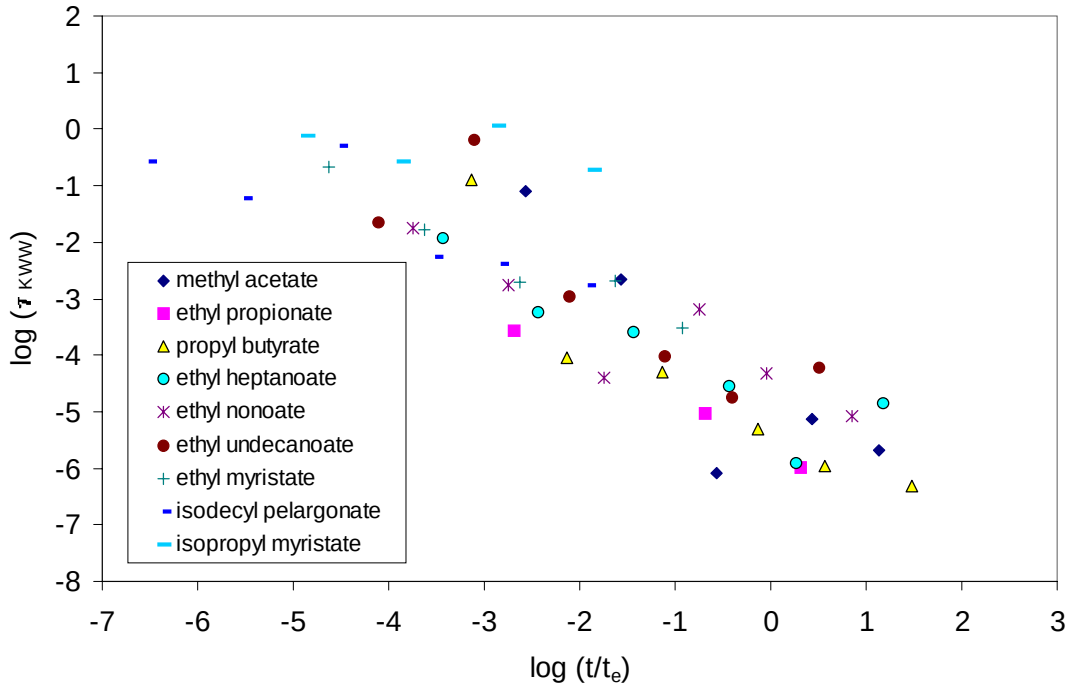

Figure 6-39. Evaluated KWW tau as a function of normalized time for polymer adhesive exposed to ester penetrants.

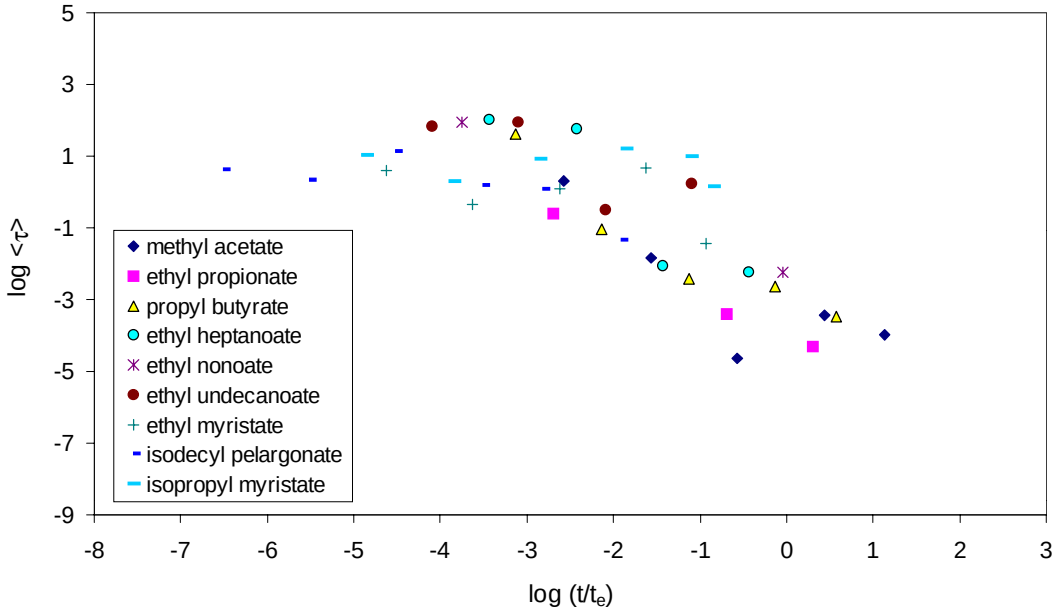

Figure 6-40. Evaluated mean relaxation time, < tau>, as a function of normalized time for polymer adhesive exposed to ester penetrants.

6.7 Summary

In this chapter, the concept of frequency-temperature superpositioning has been employed to create master curves of dynamic loss moduli versus frequency data. Temperature shift factor plots depicting the temperature dependence of the relaxation process were constructed from the master curves. These temperature shift factors provided a means of predicting the viscoelastic response of the system under different conditions of frequency and temperature. Accelerated testing of this nature is based upon the premise that the *mechanism* of the relaxation process is unaffected by changes in temperature. Then, the *shifts* associated with each isothermal curve is attributed to an increase or decrease in the *rate* of the process due to thermal changes.

Comparison of the frequency-temperature master curves of various penetrants at corresponding exposure times led to the concept of a double-reduction in variables. A newly developed shift factor designated as a *diffusion-time shift factor* ($\log a_{Dt}$), has been incorporated to describe the transport phenomenon and the effects of a penetrant on the polymer relaxation process. Diffusion-time shift factors for both esters and alkanes *increased* as a function of log (exposure time). The increasing values of $\log a_{Dt}$ reflected the shifts in the relaxation spectra to higher frequencies (i.e. lower temperatures). Normalization of the time axis by the respective equilibrium diffusion times for each penetrant resulted in a single curve for each of the penetrant series. This behavior fortified the idea that the mechanism of mechanical relaxation remained unchanged during the transport process for both the esters and *n*-alkanes. However, the rate of relaxation varied depending upon the chemical structure of the penetrants.

This double-reduction in dynamic mechanical data resulted in the consolidation of over 50 individual master curves into two single curves, one each for the *n*-alkane and ester series of penetrants. These single curves for the alkanes and esters differ slightly from each other due to the differences in diffusion rate and plasticizing efficiency between the two series.

Empirical models such as the Havriliak-Negami and the Kohlrausch-Williams-Watts function have been directly fit to experimental data. These models have been used in conjunction with one another to evaluate well-known quantities from modulus-frequency data. The concept of cooperativity has been investigated in view of the discussion on transport properties. Slight changes in the distribution of relaxation times have been attributed to the presence or absence of homogeneities in penetrant dispersion throughout the polymer matrix. Analysis of these distributions in terms of the KWW τ_{KWW} and the mean relaxation time, $\langle\tau\rangle$, has provided a physical description of the effects of penetrant within a polymer matrix on the dynamic relaxation process. Values obtained for these τ's supported the assumption of an invariant relaxation mechanism that was used in the double-reduction procedure. Thus, the existence of the diffusing molecule only aided in accelerating this relaxation mechanism.

The temperature-frequency shift factors in conjunction with the diffusion-time shift factors allowed for a means of predicting dynamic mechanical response as a function of two independent variables - temperature and exposure time. In the next chapter, this ability is further expanded by incorporation of the concepts established in the diffusion study of Chapter 4.

Endnotes

[1] M.L. Williams, R.F. Landel, and J.D. Ferry, *Journal of American Chemical Society*, 77, 3701 (1955).
[2] A.V. Tobolsky, Properties and Structure of Polymers, John Wiley Intersciences, New York, (1960).
[3] L.E. Nielson, Mechanical Properties of Polymers, Reinhold, New York, (1962).
[4] J.D. Ferry, Viscoelastic Properties of Polymers, 2nd ed., John Wiley Interscience, New York (1970).
[5] J.J. Aklonis and W.J. MacKnight, Introduction to Polymer Viscoelasticity, 2nd ed., Wiley-Science Publication, New York. (1983).
[6] F. Povolo and N. Fontelos, "Procedure to Determine if a Set of Experimental Curves are Really Related by Scaling," *Res Mechanica*, 22, 185-198 (1987).
[7] Y. Diamant and M. Folman, *Polymer*, 20, 1025-1033 (1979).
[8] M. Sumita, T.Shizuma, K. Miyasaka, and K. Ishikawa, *Journal of Macromolecular Science and Physics*, B22(4), 601-618 (1983).
[9] S. Onogi, K. Sasaguri, T. Adachi, and S. Ogihara, "Time-Humidity Superposition in Some Crystalline Polymers," *Journal of Polymer Science*, 58, *1-17 (1962).*
[10] I. Emri and V. Pavsek, "On the Influence of Moisture on the Mechanical Properties of Polymers," *Materials Forum*, 16, 123-131 (1992).
[11] M.I. Kohan, Nylon Plastics, Wiley Interscience, New York, 1973.
[12] A. Schausberger and I.V. Ahrer, *Macromolecular Chemical Physics*, 196, 2161-2172 (1995).
[13] H. Fujita and A. Kishimoto, *Journal of Chemical Physics*, 34, 393-402 (1961).
[14] N.E. Shepherd and J.P. Wightman, "Measuring and Predicting Sealant Adhesion," *Ph.D. Dissertation at Virginia Polytechnic Institute and State University*, (1995).
[15] P.C. Hiemenz, Polymer Chemistry: The Basic Concepts, Marcell Dekker, Inc., New York, 1984.
[16] P. Hevdig, Dielectric Spectroscopy of Polymers, Adam Hilger, Bristol, UK, 1977.
[17] T. Park, *Dielectric Relaxation Behavior of Poly(3-hydroxybutyrate),* Ph.D. Dissertation at Virginia Polytechnic and State University, 1994.
[18] P. Debye, *Polar Molecules*, Dover, New York, 1929.
[19] K.S. Cole and R.S. Cole, *Journal of Chemical Physics*, 9, 341 (1941).
[20] D.W. Davidson and R.S. Cole, *Journal of Chemical Physics*, 19, 1483 (1951).
[21] S. Havriliak and S. Negami, *Polymer*, 8,161 (1967).
[22] D. Boese and F. Kremer, "Molecular Dynamics in Bulk *cis*-Polyisoprene As Studied by Dielectric Spectroscopy," *Macromolecules*, 23, 829-835 (1990).
[23] S. Havriliak and S.J. Havriliak, *Polymer*, 33, 938 (1992).
[24] D. Ferri and M.Laus, *Macromolecules*, 30, 6007 (1997).
[25] G. Williams and D.C. Watts, *Transactions of the Faraday Society*, 66, 80 (1970).
[26] R.H. Cole, *Journal of Chemical Physics*, 42, 637 (1965).
[27] T.H. Nee and R.J. Zwanzig, *Journal of Chemical Physics*, 52, 6353 (1970).
[28] F. Kohlrausch, *Pogg. Ann. Physik*, 29, 337 (1863).
[29] C.P. Lindsey and G.D. Patterson, *Journal of Chemical Physics*, 73, 3348 (1980).
[30] C.M. Roland and K.L. Ngai, "Segmental Relaxation and the Correlation of Time and Temperature Dependencies in Poly(vinyl methyl ether)/Polystyrene Mixtures," *Macromolecules*, 25, 363-367 (1992).
[31] M.Connolly, F. Karasz, and M. Trimmer, "Viscoelastic and Dielectric Relaxation Behavior of Substituted Poly(*p*-phenylenes)," *Macromolecules*, 28, 1872-1881 (1995).
[32] L.C.E. Struik, Physical Aging in Amorphous Polymers and other Materials, TNO Communication No. 565, Delft, Netherlands, 1977.
[33] K.L. Ngai and C.M. Roland, "Chemical Structure and Intermolecular Cooperativity: Dielectric Relaxation Results," *Macromolecules*, 26, 6824-6830 (1993).
[34] C.P. Lindsey and G.D. Patterson, *Macromolecules*, 14, 83 (1981).
[35] A.V. Tobolsky and J.R. McLoughlin, *Journal of Polymer Science*, 8, 543 (1952).
[36] F.R. Schwarzl, Encyclopedia of Polymer Science, 17, 587-665 (19 ????).
[37] T.C. Ward, *personal communications*.
[38] G.C. Papanicolaou and C. Baxenvanakis, "Viscoelastic Modelling and Strain-Rate Behavior of Plasticized Poly(vinyl chloride), *Polymer*, 4, 4323-4329 (1991).

[39] Y.Liu, A.K. Roy, A.A. Jones, P.T. Inglefield, and P. Ogden, "An NMR Study of Plasticization and Antiplasticization of a Polymeric Glass,"*Macromolecules*, 23, 968-977 (1990).
[40] N.G. McCrum, B.E. Read, and G. Williams, Anelastic and Dielectric Effects in Polymeric Solids, Dover Publications, New York, 1967.
[41] Y. Ishida, M. Matsuo and K. Yamafuji, *Kolloid Z*, 180, 108-117 (1962).
[42] P.W. Atkins, Physical Chemistry, 4th ed., W.H. Freeman and Co., New York, 1990.
[43] J.M. Crissman and G.B. McKenna, "Physical and Chemical Aging in PMMA and Their Effects on Creep and Creep Rupture Behavior," *Journal of Polymer Science: Part B: Polymer Physics*, 28, 1463-1473 (1990).
[44] D.J. Plazek and K.L. Ngai, "Correlation of Polymer Segmental Chain Dynamics with Temperature-Dependent Time-Scale Shifts," *Macromolecules*, 24, 1222-1224 (1991).
[45] S. Matsuoka, Relaxation Phenomena in Polymers, Oxford University Press, New York 1986.
[46] K.L. Ngai, "Temperature Dependence of the Stretched Exponent in Structural Relaxation of Fragile Glass-Forming Molecular Liquids," *Journal of Non-Crystalline Solids*, 131-133, 80-93 (1991).
[47] C.A. Angell, "Relaxation in Liquids, Polymers, and Plastic Crystals- Strong/Fragile Patterns and Problems," *Journal of Non-Crystalline Solids*, 131-133, 13-31 (1991).
[48] C.M. Roland and K.L. Ngai, "Constraint Dynamics and Chemical Nature," *Journal of Non-Crystalline Solids*, 172-174, 868-875 (1994).
[49] K.L. Ngai and C.M. Roland, "Intermolecular Cooperativity and the Temperature Dependence of Segmental Relaxation in Semicrystalline Polymers," *Macromolecules*, 26, 2688-2690 (1993).